TECTONICS, VOL. 19, NO. 4, PAGES 762-786 AUGUST 2000

The recent (upper Miocene to Quaternary) and present tectonic stress distributions in the Iberian Peninsula

M. Herraiz,[1] G. De Vicente,[2] R. Lindo-Ñaupari,[1] J. Giner,[3] J. L. Simón,[4]
J. M. González-Casado,[3] O. Vadillo,[1] M. A. Rodríguez-Pascua,[2] J. I. Cicuéndez,[1]
A. Casas,[4] L. Cabañas,[1] P. Rincón,[2] A. L. Cortés,[4] M. Ramírez,[5] and M. Lucini[6]

Abstract. A general synthesis of the recent and present stress situation and evolution in the Iberian Peninsula was obtained from microstructural and seismological analysis. The stress evolution was deduced from (1) fault population analysis (FPA) from 409 sites distributed throughout the Iberian Peninsula, (2) paleostress indicators given by 324 stations taken from the bibliography, and (3) seismic data corresponding to 161 focal mechanisms evenly spread in the studied region. The application of FPA together with the determination of stress tensors and focal mechanisms for the whole Iberian microplate has provided two main results: (1) the Iberian Peninsula is undergoing a NW-SE oriented compression, except for the northeastern part (Pyrenees, Ebro Basin, and Iberian Chain), where it is N-S to NE-SW, and the Gulf of Cádiz, where it seems to be E-W, and (2) the main trends of the stress field have remained almost constant since the upper Miocene. The analysis performed by zones suggests the presence of local heterogeneities in the stress field.

1. Introduction

Since the beginning in 1986 of the World Stress Map Project (WSM), increased efforts have been made in order to collect and interpret data about the orientation and magnitude of the present stress field in different tectonic environments all over the world [*Zoback*, 1992]. In the case of Europe the studies have allowed a progressive understanding of the acting stresses on the frame of the continent [*Müller et al.*, 1992] and on some particular zones: central Europe [*Grünthal and Stromeyer*, 1992], the Mediterranean area [*Jackson and McKenzie*, 1988; *Rebaï et al.*, 1992], Fennoscandia [*Gregersen*, 1992], France [*Delouis et al.*, 1993], Portugal [*Ribeiro et al.*, 1996], western Europe [*Müller et al.*, 1997], etc. In this context, the general trend of the maximum horizontal stress $S_{H\max}$ is NW-SE to NNW-SSE, but this orientation is locally deflected by major geological structures [*Müller et al.*, 1992].

In the case of the Spanish peninsular territory the available information of WSM in 1995 was very scarce. Some data were already found by *Mezcua et al.* [1984], *Vidal* [1986], *Udías and Buforn* [1991], *Philip et al.* [1991], *Olivera et al.* [1992], the seismotectonic map of the Iberian Peninsula, the Baleares and Canary Islands [*Instituto Geográfico Nacional (IGN)*, 1992], *Grellet et al.* [1993a,b], and *Galindo-Zaldívar et al.* [1993, 1999]. In this context, in November 1995 the Sigma Project was launched with the primary aim of assessing the recent (upper Miocene-Quaternary) and current stress states in the Iberian Peninsula [*Herraiz et al.*, 1998]. The study ended in April 1998 and, according to previous works [*De Vicente et al.*, 1996; *Herraiz et al.*, 1996], adopted a methodology that used both fault population and focal mechanisms analysis. The application to a large sample of seismic and geological data has allowed us to estimate the stress field acting from the upper Miocene.

In this paper we describe the methodology and the main results of the Sigma Project concerning the recent and present regional stress distributions for continental Spain. The regional stress state is defined as the "dominant" state at the scale of hundreds of kilometers. To extend the evaluation to the whole Iberian Peninsula, the results obtained by *Ribeiro et al.* [1996] for Portugal have been also incorporated in the analysis.

2. Data

Several different techniques can be used to obtain the tectonic stress state in an area. Among them, those founded on the simultaneous application of fault population analysis and fault plane solutions analysis are particularly useful when the data samples are large. These methods are complementary because they allow a direct checking of the results from geological and geophysical analysis.

In this study, the geological information collected to draw the recent stress map was based on 733 stations: 409 stations are sites where the tectonic mesostructures and microstructures were measured and analyzed in order to obtain the stress tensor, and 324 stations reflect tectonic information from the bibliography. The main structures analyzed were faults and slip striations. The fieldwork has provided a total number of 8770 fault/striae pairs, and 8165 from them have been used to calculate 474 stress tensors. The geological stations have a heterogeneous spatial distribution because the Cenozoic rocks are also irregularly spread throughout the Spanish territory of the Iberian Peninsula. The data cover nearly 75% of the area of interest. Their main characteristics are summarized in Tables 1 and 2. The data quality has been evaluated introducing a parameter Q defined as:

[1] Departamento de Geofísica y Meteorología, Facultad de Ciencias Físicas, Universidad Complutense de Madrid, Spain.
[2] Departamento de Geodinámica, Facultad de Ciencias Geológicas, Universidad Complutense de Madrid, Spain.
[3] Departamento de Química Agrícola, Geología y Geoquímica, Universidad Autónoma de Madrid, Spain.
[4] Departamento de Geología, Universidad de Zaragoza, Zaragoza, Spain.
[5] Consejo de Seguridad Nuclear, Madrid, Spain.
[6] Empresa Nacional de Residuos Radiactivos, Sociedad Anónima, Madrid, Spain.

Copyright 2000 by the American Geophysical Union.

Paper number 2000TC900006.
0278-7407/00/2000TC900006$12.00

Table 1. Results of Fault Population Analysis With the Reches Method

Lat,deg	Lon,deg	*N*	DA	σ_1	σ_2	σ_3	*R*	S_{Hmax}	T	*Q*	Lat,deg	Lon,deg	*N*	DA	σ_1	σ_2	σ_3	*R*	S_{Hmax}	T	*Q*
43.53	-8.12	16	PUM	65/131	23/311	06/041	0.43	137	E	2	39.98	-6.53	5	M	81/376	02/106	07/196	0.24	108	E	1
43.68	-7.46	10	M	65/206	18/022	15/113	0.02	63	E	2	43.39	-4.57	15	M	00/316	16/046	73/226	0.25	136	C	2
43.68	-7.46	15	M	79/220	03/129	09/038	0.22	126	E	2	43.39	-4.38	10	M	31/362	47/182	24/088	0.16	139	SS	1
43.45	-7.88	31	PUM	85/220	01/310	04/040	0.07	132	E	3	43.39	-4.33	6	UM	68/060	17/231	11/325	0.40	60	E	2
43.14	-8.30	38	M	85/139	02/319	04/049	0.12	141	E	2	43.39	-4.33	9	UM	05/330	76/062	11/239	0.16	150	SS	1
43.10	-8.26	7	M	46/195	36/292	19/080	0.10	147	SS	2	43.95	-4.41	28	M	79/177	00/085	10/352	0.18	85	E	2
43.07	-8.21	14	M	83/240	03/058	05/148	0.27	57	E	2	43.95	-4.41	40	M	09/178	57/085	30/274	0.17	179	SS	2
43.05	-8.21	21	PUM	89/140	00/307	00/037	0.18	128	E	3	43.38	-4.51	20	M	86/359	00/268	03/178	0.25	88	E	2
43.03	-8.15	26	PUM	82/194	04/104	05/023	0.13	101	E	2	43.38	-4.44	13	M	75/267	14/087	02/357	0.39	87	E	2
42.85	-7.37	19	PUM	82/236	05/146	05/050	0.11	151	E	2	43.38	-4.44	22	M	03/202	44/109	44/285	0.37	23	SS	3
42.87	-7.37	13	M	81/229	02/323	08/054	0.14	147	E	2	43.36	-4.42	10	M	09/115	35/023	52/208	0.68	121	C	2
42.86	-7.16	7	PUM	69/068	20/243	01/333	0.37	64	E	1	43.37	-4.48	7	M	02/251	41/340	48/159	0.03	72	SS	1
42.86	-7.16	15	PUM	36/240	52/156	05/060	0.28	146	SS	2	43.37	-4.48	7	M	26/342	17/071	56/248	0.23	159	C	1
42.84	-7.18	11	PUM	83/195	04/007	04/092	0.75	8	E	1	43.39	4.39	20	M	02/128	17/219	72/030	0.06	129	C	3
42.83	-7.22	14	PUM	48/304	41/126	00/032	0.40	125	SS	2	43.39	4.39	16	M	68/221	07/124	20/031	0.10	128	E	3
42.83	-7.22	12	PUM	36/240	53/069	04/334	0.95	70	SS	1	43.20	-5.33	5	M	58/301	31/122	01/031	0.19	120	E	0
42.73	-6.58	15	PUM	33/156	10/065	54/330	0.19	165	C	2	43.24	-5.38	18	M	81/296	01/029	08/119	0.14	32	E	3
42.73	-6.58	7	PUM	02/125	37/217	52/040	0.18	126	C	1	43.15	-5.27	29	M	32/046	57/222	02/315	0.68	46	SS	2
42.76	-6.62	21	PUM	74/340	09/077	11/169	0.25	86	E	2	43.06	-5.14	15	M	24/128	59/308	15/219	0.84	129	SS	1
42.56	-7.49	15	M	05/067	00/156	86/248	0.79	67	C	3	43.06	-5.14	10	M	04/252	85/050	01/162	0.40	73	SS	2
42.53	-7.49	22	PUM	02/319	05/049	83/138	0.89	137	C	4	42.88	-5.45	20	M	85/179	02/278	03/008	0.15	100	E	2
42.64	-6.56	7	PUM	07/295	18/200	70/020	0.18	116	C	2	42.99	-5.00	14	M	73/211	02/301	16/032	0.69	123	E	2
42.58	-6.56	7	M	82/263	02/176	07/085	0.96	176	E	1	42.99	-5.00	15	M	06/196	74/289	13/105	0.27	17	SS	2
42.52	-6.63	18	PUM	72/028	16/203	04/294	0.30	23	E	2	42.89	-4.75	22	M	86/342	00/071	03/161	0.60	71	E	3
42.52	-6.63	20	PUM	78/048	00/150	11/240	0.86	150	E	1	42.89	-4.75	13	M	63/145	25/319	06/050	0.56	142	E	2
42.52	-6.63	18	PUM	12/319	67/052	18/225	0.84	136	SS	2	42.88	-4.70	15	M	83/316	06/136	02/046	0.57	136	E	2
42.51	-6.54	22	PUM	27/159	50/250	26/054	0.62	151	SS	1	42.80	-5.65	7	M	84/168	03/078	04/348	0.04	71	E	2
42.44	-7.04	14	M	66/171	23/355	01/265	0.09	173	E	2	42.79	-5.74	8	M	63/323	02/053	26/145	0.16	49	E	1
42.44	-7.02	15	M	77/192	10/023	07/291	0.09	10	E	2	42.79	-5.74	7	M	26/017	13/287	60/195	0.79	20	C	1
42.42	-6.93	17	M	70/178	18/016	05/284	0.70	14	E	2	42.80	-5.67	6	M	75/280	12/084	08/175	0.21	92	E	1
42.45	-6.97	34	M	76/085	05/276	11/184	0.05	96	E	2	42.80	-5.67	6	M	07/163	72/258	15/071	0.45	163	SS	1
42.46	-6.94	20	PUM	79/076	10/256	00/346	0.17	77	E	4	42.53	-5.98	9	Q	89/240	00/060	00/150	0.07	60	E	4
42.43	-6.98	12	PUM	78/150	08/320	07/051	0.32	144	E	2	40.75	-3.03	30	PUM	85/318	00/223	04/133	0.01	42	E	2
42.42	-6.82	11	M	19/118	70/299	00/208	0.59	119	SS	1	40.75	-3.03	28	PUM	09/332	76/159	10/064	0.45	153	SS	2
42.48	-6.79	6	M	16/084	70/269	10/177	0.29	85	SS	1	40.58	-3.08	21	PUM	82/051	06/240	04/149	0.86	59	E	2
42.48	-6.79	20	M	04/337	84/67	02/247	0.63	157	SS	2	40.58	-3.08	22	PUM	84/330	04/146	02/236	0.61	147	E	2
42.29	-7.59	15	M	87/117	02/313	00/223	0.26	134	E	2	40.60	-2.72	13	Q	18/077	70/249	05/347	0.72	76	SS	3
42.01	-7.89	19	M	01/081	84/345	05/171	0.87	81	SS	2	40.60	-2.72	8	Q	43/312	45/128	05/220	0.48	137	SS	2
42.07	-7.68	22	M	87/259	02/075	01/165	0.37	76	E	2	40.55	-2.75	9	PUM	00/312	76/042	13/222	0.28	133	SS	2
42.13	-7.75	20	M	85/227	03/049	01/319	0.72	49	E	2	40.55	-2.75	7	PUM	77/232	11/052	05/321	0.07	41	E	2
42.05	-6.64	28	M	74/095	12/279	08/187	0.07	87	E	2	40.51	-2.77	11	PUM	78/198	11/017	01/107	0.48	18	E	2
41.85	-7.39	7	M	63/196	04/296	25/029	0.06	116	E	0	40.64	-2.50	22	PUM	15/327	72/145	06/236	0.58	147	SS	2
41.86	-7.43	13	M	59/231	28/072	08/337	0.68	66	E	2	40.42	-3.57	30	UM	86/131	02/041	02/311	0.08	41	E	3
41.85	-7.44	19	M	75/343	13/170	04/079	0.28	168	E	1	40.45	-3.12	50	PUM	86/236	03/056	00/146	0.23	57	E	2
41.93	-7.50	30	M	78/238	11/054	00/144	0.21	55	E	2	40.45	-3.12	29	PUM	43/144	45/324	08/055	0.20	151	SS	2
41.94	-7.50	33	M	86/079	03/169	00/259	0.11	170	E	2	40.38	-3.11	39	UM	81/172	04/271	06/002	0.10	97	E	3
41.95	-7.45	17	M	81/245	08/063	02/153	0.54	64	E	2	40.41	-3.05	16	PUM	20/209	05/301	69/041	0.34	28	C	2
43.60	-5.93	8	M	11/159	15/066	69/253	0.12	160	C	1	40.42	-2.91	10	PUM	84/055	02/146	04/237	0.86	147	E	2
43.39	-6.33	11	PUM	13/134	06/042	74/234	0.36	133	C	2	40.42	-2.91	15	PUM	86/029	03/209	02/119	0.46	29	E	2
43.39	-5.58	18	M	05/235	64/335	25/143	0.36	55	SS	2	40.47	-2.95	20	PUM	82/057	02/327	07/237	0.43	147	E	2
43.39	-5.58	7	M	02/160	07/251	81/075	0.13	161	C	1	40.47	-2.95	8	PUM	44/219	44/039	03/125	0.57	37	SS	1
43.39	-5.58	10	PUM	72/210	16/033	04/302	0.32	30	E	2	40.47	-2.78	40	Q	86/312	02/222	02/132	0.23	42	E	2
40.27	-3.53	16	Q	78/124	03/230	10/321	0.05	53	E	3	40.47	-2.78	31	Q	79/154	10/334	02/064	0.20	156	E	3
40.26	-3.53	5	Q	76/198	11/024	06/293	0.28	20	E	1	38.72	-0.45	10	Q	86/173	03/357	00/267	0.14	177	E	2
40.28	-3.38	20	PUM	18/061	71/235	04/329	0.66	60	SS	3	38.72	-0.47	14	PUM	87/054	00/144	01/234	0.79	144	E	2
40.28	-3.38	20	PUM	00/140	82/232	07/049	0.39	140	SS	2	38.74	-0.47	9	PUM	71/049	11/318	14/228	0.20	127	E	1
40.24	-3.35	10	PUM	03/244	83/130	05/334	0.60	65	SS	1	38.74	-0.47	14	PUM	04/139	75/048	13/230	0.61	140	SS	1

Table 1. (continued)

Lat,deg	Lon,deg	N	DA	σ_1	σ_2	σ_3	R	S_{Hmax}	T	Q	Lat,deg	Lon,deg	N	DA	σ_1	σ_2	σ_3	R	S_{Hmax}	T	Q
40.23	-3.46	16	PUM	37/235	52/051	02/144	0.92	54	SS	2	38.09	-0.49	14	PUM	86/137	03/317	00/227	0.02	137	E	2
40.23	-3.41	16	PUM	86/220	03/045	00/315	0.09	45	E	1	38.74	-0.45	20	M	71/309	13/129	11/219	0.26	141	E	2
40.23	-3.46	20	PUM	87/047	01/137	02/227	0.12	138	E	2	38.74	-0.46	18	PUM	82/336	00/245	07/159	0.14	69	E	2
40.18	-3.04	10	Q	86/132	01/243	03/334	0.07	63	E	2	38.73	-0.45	12	PUM	83/069	06/251	01/161	0.14	70	E	2
40.18	-3.04	14	Q	15/196	02/105	74/016	0.87	20	C	2	38.72	-0.48	7	PUM	88/198	00/018	00/108	0.63	18	E	2
40.19	-3.03	13	Q	86/032	03/237	01/147	0.11	57	E	2	38.77	-0.47	30	PUM	75/146	14/326	00/236	0.16	146	E	4
40.24	-2.84	12	UM	79/137	08/047	05/316	0.30	45	E	2	38.75	-0.45	20	PUM	76/045	08/316	10/226	0.09	121	E	2
40.24	-2.84	7	UM	17/326	19/062	63/152	0.77	131	C	1	38.75	-0.45	8	PUM	42/294	34/165	28/053	0.81	140	SS	1
40.28	-2.84	30	PUM	12/335	75/129	06/243	0.95	154	SS	2	38.70	-0.34	21	PUM	81/129	03/308	07/038	0.06	139	E	3
40.28	-2.84	8	PUM	81/100	05/210	06/301	0.43	32	E	2	38.74	-0.27	10	Q	29/251	53/151	19/342	0.52	78	SS	2
40.29	-2.84	20	PUM	78/050	06/141	09/233	0.70	144	E	2	38.83	0.00	20	Q	76/193	02/104	13/014	0.05	100	E	2
40.29	-2.84	8	PUM	47/227	38/020	16/118	0.42	36	SS	1	38.64	-2.44	16	Q	02/325	24/234	65/055	0.43	146	C	2
40.13	-3.84	27	UM	87/132	01/041	02/311	0.04	40	E	3	38.64	-2.44	15	Q	75/125	13/035	06/305	0.19	31	E	2
40.05	-3.77	20	UM	83/055	05/230	03/320	0.11	53	E	2	38.66	-2.41	28	Q	23/156	55/065	24/247	0.10	158	SS	2
40.07	-3.73	21	UM	80/168	09/345	02/075	0.02	170	E	2	38.62	-2.49	9	PUM	00/276	86/007	03/185	0.09	96	SS	2
40.13	-2.91	10	Q	84/344	04/074	04/165	0.07	79	E	2	38.62	-2.49	20	PUM	09/343	45/073	42/253	0.29	153	SS	2
40.17	-3.09	9	Q	32/228	56/040	08/136	0.56	49	SS	2	38.55	-2.38	25	M	80/120	01/210	09/300	0.34	31	E	2
40.17	-3.09	20	Q	86/144	03/324	01/054	0.35	145	E	1	38.58	-2.40	28	M	01/124	19/215	70/034	0.21	124	C	3
40.12	-2.56	20	PUM	07/239	43/340	45/149	0.15	58	C	2	38.59	-2.44	12	M	26/067	08/158	61/248	0.61	52	C	2
40.12	-2.56	11	PUM	78/260	10/054	05/145	0.24	58	E	2	38.59	-2.44	12	M	23/302	66/122	03/032	0.56	122	SS	2
40.18	-2.69	6	Q	80/119	08/291	04/022	0.17	115	E	1	38.63	-2.30	14	M	14/046	63/138	21/316	0.43	45	SS	2
39.87	-3.03	16	PUM	85/132	00/225	03/315	0.14	46	E	2	38.63	-2.30	8	M	10/111	77/202	06/020	0.18	112	SS	0
39.30	-1.34	19	PUM	01/321	67/229	22/052	0.27	142	SS	2	38.52	-2.51	23	M	56/038	06/127	33/232	0.12	120	E	1
38.93	-4.04	12	Q	80/013	09/193	00/103	0.79	14	E	2	38.59	-2.17	14	M	04/122	84/303	02/212	0.44	123	SS	2
38.97	-3.99	20	PUM	60/060	28/243	03/152	0.65	63	SS	1	38.59	-2.17	12	M	84/053	04/233	02/143	0.46	53	E	2
38.97	-3.99	11	PUM	03/333	86/150	00/243	0.80	153	C	2	38.60	-2.14	13	M	82/224	06/134	02/044	0.24	134	E	2
38.98	-4.05	39	Q	24/147	63/339	08/241	0.46	150	SS	2	38.60	-2.14	20	M	06/096	83/276	00/186	0.08	96	SS	3
38.89	-3.65	45	PUM	80/222	09/048	00/318	0.60	48	E	2	38.60	-2.14	9	M	82/215	01/125	07/034	0.11	123	E	1
38.89	-3.65	32	PUM	79/146	10/324	01/055	0.76	145	E	3	38.60	-2.12	16	M	07/263	52/174	36/353	0.31	83	SS	2
38.91	-3.70	30	PUM	22/046	67/220	03/314	0.76	48	SS	2	38.60	-2.12	8	M	10/151	39/060	49/241	0.15	160	C	3
38.91	-3.70	23	PUM	17/332	72/153	02/063	0.95	154	SS	3	38.57	-2.07	10	M	18/320	38/050	45/226	0.15	140	C	1
38.84	-3.67	50	PUM	83/220	06/032	02/123	0.31	32	E	2	38.57	-2.07	14	M	86/205	03/025	01/295	0.44	25	E	1
38.84	-3.67	20	PUM	06/042	36/137	52/309	0.03	43	C	1	38.55	-2.08	14	M	64/326	23/145	08/055	0.56	143	E	2
38.84	-3.67	25	PUM	35/333	53/156	05/067	0.88	153	SS	2	38.55	-2.08	12	M	76/125	11/035	07/305	0.34	31	E	2
38.84	3.61	30	PUM	79/128	10/307	01/037	0.47	128	E	1	38.55	-2.11	26	M	43/024	45/202	08/293	0.65	32	SS	3
38.84	3.61	22	PUM	88/049	01/231	00/141	0.35	52	E	3	38.56	-2.01	17	PUM	78/265	09/082	06/352	0.25	82	E	2
38.81	-4.11	34	PUM	67/039	20/211	06/303	0.41	37	E	2	38.73	-2.01	19	Q	80/324	09/143	04/234	0.09	143	E	2
38.81	-4.11	30	PUM	81/178	07/269	01/005	0.62	90	E	3	38.50	-1.66	10	Q	05/221	81/262	06/040	0.43	41	SS	1
38.83	-3.75	39	PUM	84/247	04/043	02/133	0.65	44	E	4	38.53	-0.08	13	PUM	80/217	06/307	06/037	0.21	131	E	1
38.83	-3.75	39	PUM	05/320	84/143	01/230	0.72	140	SS	2	38.47	-2.54	12	M	80/326	08/145	04/236	0.67	145	SS	2
38.77	-3.78	60	PUM	79/232	05/052	08/142	0.72	53	E	2	38.47	-2.54	17	M	40/238	48/044	06/142	0.50	45	SS	2
38.77	-3.78	30	PUM	87/318	02/136	00/226	0.82	137	E	3	38.45	-2.69	20	M	21/142	67/322	04/052	0.55	144	SS	2
39.25	-0.55	8	PUM	74/143	13/327	07/235	0.33	142	SS	1	38.45	-2.69	21	M	74/310	11/220	10/130	0.36	37	E	1
39.25	-0.55	8	PUM	37/053	52/222	05/319	0.39	51	SS	1	38.48	-2.45	17	M	86/291	03/093	01/183	0.49	93	E	2
39.28	-0.57	32	Q	75/168	14/341	01/072	0.60	162	E	2	38.48	-2.45	15	M	83/107	001/00	06/270	0.44	1	E	2
39.00	-0.29	15	Q	84/313	00/044	05/134	0.21	45	E	3	38.48	-2.42	16	M	72/208	17/038	02/307	0.34	36	E	2
38.72	-0.46	9	PUM	70/089	18/265	05/356	0.43	89	E	1	38.48	-2.42	10	M	71/160	16/313	07/045	0.62	137	E	1
38.49	-2.32	15	M	81/153	05/333	06/242	0.59	152	E	1	38.49	-2.32	18	M	65/317	24/134	01/224	0.32	135	E	2
38.48	-2.18	6	PUM	24/085	12/349	61/179	0.09	86	C	1	37.54	-3.11	20	Q	06/232	03/142	82/023	0.11	53	C	2
38.48	-2.18	15	PUM	07/325	33/233	54/060	0.59	149	C	2	37.54	-3.11	16	Q	03/152	83/062	05/243	0.42	153	SS	2
38.46	-2.14	36	PUM	09/290	80/112	01/020	0.39	111	SS	2	37.21	-4.29	11	PUM	30/162	59/341	01/071	0.28	162	SS	2
38.46	-2.05	16	M	16/202	69/292	11/111	0.34	24	SS	2	37.26	-4.31	36	PUM	72/113	15/293	02/023	0.24	119	E	2
38.46	-2.05	15	M	11/305	78/144	03/035	0.04	125	SS	2	37.27	-4.38	13	PUM	65/174	23/011	06/278	0.66	8	E	1
38.45	-2.07	18	M	11/143	70/050	14/236	0.45	143	SS	2	37.06	-5.81	24	Q	04/302	76/032	12/211	0.33	122	SS	2
38.45	-2.07	8	M	19/222	70/049	02/313	0.47	45	SS	2	37.03	-4.53	16	M	75/046	03/306	13/215	0.04	126	E	2
38.42	-2.03	22	M	18/200	18/293	63/025	0.18	12	C	1	37.03	-4.57	17	PUM	08/187	49/277	38/097	0.32	6	SS	2
38.47	-2.17	23	PUM	01/207	86/297	02/117	0.52	27	SS	2	37.03	-4.60	21	PUM	01/183	22/093	67/273	0.19	4	C	2
38.47	-2.17	20	PUM	86/069	02/247	01/337	0.15	67	E	2	37.14	-4.72	11	PUM	80/214	09/033	02/124	0.27	35	E	2

Table 1. (continued)

Lat,deg	Lon,deg	N	DA	σ_1	σ_2	σ_3	R	S_{Hmax}	T	Q	Lat,deg	Lon,deg	N	DA	σ_1	σ_2	σ_3	R	S_{Hmax}	T	Q
38.46	-1.94	29	PUM	83/066	05/245	03/336	0.31	65	E	2	37.15	-4.52	6	PUM	05/343	83/125	04/253	0.43	163	SS	0
38.46	-1.94	7	PUM	14/039	13/306	69/129	0.09	40	C	0	36.89	-5.59	8	Q	84/148	03/058	03/328	0.07	55	E	2
38.47	-1.99	17	PUM	81/230	08/048	02/138	0.04	54	E	3	36.87	-5.81	34	PUM	50/149	20/333	32/239	0.12	152	E	4
38.42	-2.00	15	PUM	01/059	76/150	12/328	0.03	59	SS	3	36.99	-5.58	15	Q	77/250	05/340	10/071	0.09	160	E	3
38.46	-1.94	7	PUM	03/162	15/071	73/269	0.48	163	C	1	36.86	-6.04	27	Q	81/142	02/052	08/322	0.10	48	E	2
38.42	-2.00	13	PUM	50/293	40/118	05/028	0.39	120	SS	2	36.86	-5.19	10	PUM	59/060	02/149	30/240	0.08	149	E	2
38.41	-2.00	25	PUM	84/320	05/142	00/052	0.40	142	E	2	36.86	-5.19	8	PUM	89/180	00/091	000/01	0.17	90	E	2
38.42	-2.03	17	PUM	73/120	04/300	09/030	0.05	120	E	2	36.72	-6.03	22	PUM	76/104	02/014	13/284	0.12	10	E	2
38.48	-1.79	21	PUM	10/231	26/140	61/328	0.01	51	C	2	36.75	-5.81	7	PUM	57/095	31/274	06/004	0.34	98	E	0
38.48	-1.79	50	PUM	71/284	13/194	12/101	0.10	171	E	2	36.46	-5.93	21	Q	60/208	08/115	22/025	0.30	104	E	2
38.38	-1.76	33	PUM	05/053	00/143	84/236	0.61	54	C	3	36.34	-5.82	16	M	23/136	53/226	25/044	0.14	135	SS	2
38.38	-1.80	46	PUM	66/242	23/065	02/334	0.60	64	E	2	36.48	-5.77	14	M	80/178	08/019	04/289	0.17	15	E	2
38.34	-1.65	21	PUM	03/342	03/072	84/252	0.47	162	C	2	36.25	-5.95	8	Q	14/146	01/236	75/327	0.54	146	C	2
38.34	-1.65	10	PUM	83/269	04/089	04/180	0.34	89	E	3	36.25	-5.93	7	PUM	75/262	13/082	02/172	0.22	80	E	1
38.37	-1.67	46	PUM	03/149	24/057	65/242	0.24	150	C	3	36.20	-5.98	7	Q	12/126	72/035	12/216	0.17	127	SS	1
38.37	-1.67	60	PUM	71/140	14/049	12/316	0.20	36	E	3	36.25	-5.97	15	Q	13/201	04/110	75/020	0.37	22	C	2
38.35	-1.70	4	Q	14/156	33/059	52/246	0.17	158	C	0	37.70	-1.65	23	Q	08/355	04/086	80/265	0.14	175	C	3
38.35	-1.70	12	Q	76/009	6/270	11/179	0.06	80	E	2	37.70	-1.64	25	Q	09/353	44/083	44/264	0.24	172	SS	2
38.26	-2.78	11	M	17/298	70/110	08/206	0.18	118	SS	0	37.71	-1.64	20	Q	11/337	51/067	35/247	0.30	146	SS	2
38.26	-2.78	15	M	03/034	86/124	01/304	0.24	35	SS	2	37.71	-1.64	24	Q	66/233	22/053	04/323	0.59	64	E	2
38.28	-2.76	20	M	01/202	74/295	15/112	0.26	22	SS	2	37.71	-1.63	24	Q	01/172	02/262	87/082	0.16	172	C	2
38.28	-2.76	21	M	54/279	34/105	05/011	0.41	99	E	3	37.71	-1.62	21	Q	10/355	37/085	50/265	0.32	173	C	2
38.18	-2.80	20	M	04/260	75/355	13/162	0.38	80	SS	2	37.71	-1.61	8	Q	05/015	06/285	81/195	0.69	16	C	1
38.18	-2.80	20	M	19/179	69/357	05/087	0.65	174	SS	2	37.83	-1.79	38	M	82/163	06/343	02/073	0.11	165	E	2
38.22	-1.59	14	Q	86/349	03/171	00/081	0.05	171	E	2	37.73	-1.81	10	PUM	86/371	02/191	12/100	0.21	11	E	2
38.24	-1.72	14	PUM	80/061	09/331	01/241	0.79	151	E	2	37.38	-1.62	7	PUM	58/041	27/311	14/222	0.87	123	E	1
38.24	-1.72	9	PUM	87/225	00/131	02/041	0.09	131	E	2	37.19	-1.82	8	Q	84/243	05/063	01/333	0.19	62	E	1
38.16	-2.99	20	M	08/242	59/138	29/337	0.17	63	SS	1	37.30	-1.80	17	PUM	70/163	03/253	19/344	0.03	73	E	1
38.16	-2.99	11	M	22/134	64/320	12/229	0.28	136	SS	2	37.08	-2.07	18	PUM	80/277	03/097	09/187	0.11	92	E	2
38.01	-3.04	15	M	53/138	36/308	04/011	0.27	130	E	2	37.08	-2.07	15	PUM	08/312	74/133	12/042	0.93	134	SS	2
37.93	-2.98	31	M	44/202	44/023	08/114	0.09	31	SS	2	37.07	-2.05	13	PUM	75/234	14/054	00/324	0.12	53	E	2
37.96	-2.95	15	M	34/144	55/322	00/053	0.54	144	SS	2	37.06	-2.02	6	PUM	50/150	39/330	00/240	0.77	150	E	1
37.96	-2.95	19	M	63/048	24/230	09/139	0.40	45	E	2	37.06	-2.02	20	PUM	71/137	12/047	13/317	0.03	47	E	2
37.86	-3.04	28	M	87/311	01/131	01/221	0.84	132	E	4	37.05	-2.04	7	UM	05/127	50/040	38/217	0.13	128	SS	1
37.84	-1.42	11	PUM	50/027	37/204	10/295	0.37	31	E	2	37.05	-2.04	20	UM	25/082	55/352	21/173	0.77	88	SS	2
37.96	-1.38	11	PUM	75/116	14/297	00/206	0.20	117	E	2	37.10	-2.12	6	Q	39/151	43/261	20/061	0.28	145	SS	1
37.97	-1.30	11	M	80/090	5/179	08/270	0.27	3	E	1	37.05	-1.88	17	UM	00/144	82/234	07/054	0.88	145	SS	1
37.79	-3.05	42	M	79/195	08/012	05/102	0.79	13	E	3	37.05	-1.88	23	UM	77/052	10/232	05/141	0.27	49	E	2
37.57	-2.95	15	M	30/130	59/316	04/223	0.21	1	SS	1	37.03	-1.93	12	Pli	84/078	05/258	01/348	0.36	78	E	1
37.57	-2.95	14	M	29/271	60/088	04/178	0.95	89	SS	2	37.14	-1.85	7	PUM	15/328	51/238	34/058	0.12	149	SS	1
37.58	-3.11	25	M	55/299	33/112	09/208	0.27	124	E	2	37.14	-1.85	7	PUM	79/163	08/343	06/073	0.18	163	SS	1
37.13	-1.83	6	PUM	73/100	16/201	01/292	0.56	23	E	1	37.13	-1.83	6	PUM	69/139	24/319	00/229	0.40	139	E	1
37.09	-1.85	20	PUM	02/302	81/035	08/212	0.20	122	SS	1	40.84	1.90	10	PUM	89/260	00/350	00/080	0.01	171	E	2
37.09	-1.85	7	PUM	52/050	36/229	07/320	0.94	51	E	2	40.92	-1.27	5	Q	74/248	12/068	08/338	0.06	50	E	1
37.07	-1.85	15	M	32/131	56/310	08/041	0.64	133	SS	2	41.03	-1.28	5	Q	68/253	13/163	16/073	0.08	158	E	1
37.07	-1.85	18	M	66/095	22/283	06/190	0.16	94	E	2	40.51	0.24	18	M	78/088	02/268	11/178	0.11	81	E	2
37.16	-1.83	40	PUM	31/150	58/332	03/243	0.83	153	SS	2	40.61	0.20	35	M	81/042	07/222	03/312	0.47	43	E	2
36.94	-3.02	27	Q	54/345	33/170	09/078	0.11	159	E	3	40.36	-1.08	11	PUM	83/070	04/160	04/251	0.07	166	E	2
36.91	-3.02	16	Q	79/173	03/263	09/353	0.10	91	E	2	40.29	-0.73	23	Q	85/205	02/295	03/025	0.08	117	E	2
36.99	-2.46	17	PUM	72/308	17/124	01/214	0.30	126	E	2	40.24	0.06	33	M	82/129	06/219	04/309	0.04	40	E	3
36.85	-2.29	7	PUM	86/339	03/158	01/249	0.12	159	E	1	40.25	0.01	25	M	84/138	01/228	05/318	0.09	50	E	3
36.95	-2.20	5	Q	78/119	10/310	05/219	0.66	129	E	1	40.19	0.04	35	M	77/287	05/197	10/106	0.24	13	E	1
36.94	-1.91	40	PUM	80/319	02/224	08/134	0.05	40	E	2	40.30	0.19	13	M	06/269	34/179	58/359	0.35	91	C	1
37.00	-1.90	26	Q	10/159	69/065	17/250	0.28	161	SS	2	40.30	0.19	18	M	88/325	01/145	00/055	0.08	145	E	3
37.00	-1.90	20	Q	21/209	66/023	10/115	0.83	28	SS	2	40.06	-1.31	7	PUM	86/186	00/276	03/006	0.04	98	E	2
36.87	-2.16	10	PUM	76/278	08/184	09/093	0.09	170	E	2	41.85	-1.23	11	PUM	81/089	08/269	01/179	0.02	86	E	2
36.87	-2.15	36	Q	03/319	81/050	07/228	0.59	139	SS	2	41.84	-1.24	27	PUM	80/339	09/158	00/248	0.04	159	E	2
36.87	-2.15	30	Q	84/050	04/230	03/320	0.31	51	E	2	41.84	-1.25	11	PUM	82/071	01/160	07/250	0.03	160	E	3

Table 1. (continued)

Lat,deg	Lon,deg	*N*	DA	σ_1	σ_2	σ_3	*R*	$S_{H\max}$	T	*Q*	Lat,deg	Lon,deg	*N*	DA	σ_1	σ_2	σ_3	*R*	$S_{H\max}$	T	*Q*
36.88	-2.04	10	PUM	80/097	08/276	03/007	0.11	101	E	1	41.86	-1.20	18	PUM	82/136	06/316	03/046	0.06	143	E	2
36.88	-2.04	15	PUM	79/033	10/213	02/303	0.30	34	E	2	41.86	-1.23	9	PUM	75/262	04/172	13/081	0.10	165	E	1
37.00	-1.90	13	Q	77/175	12/001	01/270	0.57	1	E	2	39.94	-1.38	12	PUM	71/118	18/297	02/028	0.24	120	E	2
36.79	-2.96	23	Q	84/216	03/126	02/036	0.06	124	E	2	39.94	-1.38	10	PUM	73/261	13/081	09/351	0.02	80	E	2
36.82	-2.25	15	Q	83/224	06/044	00/314	0.20	44	E	2	39.73	-1.48	8	PUM	63/086	22/266	12/356	0.19	86	E	0
36.77	-2.09	20	PUM	76/121	09/031	09/220	0.05	30	E	1	39.73	-1.48	5	PUM	78/046	11/226	00/316	0.38	46	E	1
38.08	-3.99	10	M	67/336	20/151	08/244	0.40	158	E	2	39.75	-1.47	6	PUM	76/268	12/089	01/358	0.06	85	E	1
36.82	-2.25	13	Q	32/338	38/132	35/222	0.10	156	SS	1	39.72	-1.45	24	PUM	74/150	15/329	03/059	0.87	150	E	2
38.08	-3.99	20	M	73/198	15/023	04/292	0.78	22	E	3	39.55	-1.08	33	M	68/063	20/244	04/153	0.53	62	E	2
38.11	-3.94	20	M	79/205	10/024	02/115	0.43	26	E	2	39.51	-1.08	17	PUM	74/241	05/331	14/061	0.12	151	E	1
38.11	-3.94	14	M	73/319	16/140	01/049	0.70	140	E	1	39.51	-1.08	10	PUM	78/308	05/218	10/127	0.19	38	E	2
38.08	-4.17	8	Q	79/030	07/208	07/299	0.02	61	E	2	39.67	-0.60	30	PUM	85/336	04/156	00/246	0.62	151	E	3
38.17	-3.78	15	M	81/065	02/160	07/250	0.56	161	E	2	39.67	-0.60	39	PUM	67/177	19/357	09/087	0.10	16	E	2
38.17	-3.78	16	M	44/237	39/056	18/147	0.11	74	SS	2	39.51	0.05	7	PUM	61/191	27/011	07/101	0.81	12	E	1
38.11	-3.77	7	PUM	79/068	03/159	09/249	0.55	160	E	1	39.51	0.05	6	PUM	39/320	42/161	21/050	0.33	129	SS	0
38.11	-3.77	6	PUM	36/237	07/141	52/051	0.20	60	C	2	39.54	-0.44	15	PUM	75/335	14/155	00/065	0.23	155	E	2
38.09	-3.84	42	M	76/012	06/279	12/188	0.25	94	E	2	39.59	-0.42	12	PUM	67/239	21/059	03/329	0.72	58	E	2
37.38	-6.73	7	Q	86/231	03/051	00/141	0.18	52	E	1	39.61	-0.53	6	PUM	73/316	15/136	04/226	0.67	138	E	0
37.47	-5.64	17	PUM	32/222	57/042	04/133	0.28	51	SS	2	39.47	-1.71	15	PUM	06/144	82/054	04/234	0.42	145	SS	2
37.30	-7.32	14	Q	78/044	00/137	11/227	0.16	138	E	2	39.47	-1.71	16	PUM	85/231	04/051	01/321	0.20	51	E	2
37.25	-7.22	34	PUM	83/306	05/126	02/036	0.03	121	E	3	39.56	-1.05	18	PUM	13/188	59/278	26/098	0.09	185	SS	3
37.23	-7.23	24	PUM	82/300	02/032	07/123	0.05	30	E	3	39.56	-1.05	28	PUM	10/095	71/005	15/185	0.18	96	SS	2
37.23	-7.20	24	PUM	64/153	10/243	22/338	0.05	60	E	2	39.41	-0.73	43	PUM	05/033	82/214	05/124	0.60	34	SS	2
37.24	-7.22	17	PUM	89/131	00/311	00/041	0.21	132	E	2	39.44	-0.77	6	PUM	82/141	05/321	04/051	0.12	149	E	0
37.24	-7.22	33	PUM	81/321	08/143	00/053	0.06	143	E	4	42.45	-3.69	11	M	87/331	01/151	00/061	0.06	151	E	2
37.24	-7.21	36	PUM	87/309	02/128	00/218	0.03	129	E	2	42.30	-3.62	11	Q	85/183	02/273	03/003	0.02	101	E	3
37.24	-7.23	18	PUM	89/309	00/147	00/237	0.03	147	E	2	41.91	-3.73	7	PUM	87/244	00/136	02/046	0.10	137	E	2
37.24	-7.23	6	PUM	86/348	02/168	02/078	0.06	167	E	3	41.91	-3.73	10	PUM	85/300	03/120	02/210	0.32	121	E	2
37.28	-7.21	9	PUM	83/290	04/200	04/110	0.08	16	E	2	41.86	-3.58	12	Pli	79/286	07/106	07/015	0.04	109	E	2
37.23	-7.20	15	Q	47/302	42/119	03/212	0.08	127	SS	2	41.97	-3.80	7	PUM	77/194	10/284	07/015	0.31	104	E	3
41.54	-1.52	31	PUM	76/209	07/030	10/122	0.58	33	E	2	41.79	-3.53	8	PUM	86/223	02/313	02/044	0.04	137	E	1
41.61	-1.60	38	PUM	78/205	04/295	11/026	0.03	115	E	3	41.80	-3.53	12	PUM	79/083	10/262	00/352	0.03	83	E	2
41.15	-1.39	31	PUM	01/215	88/036	00/125	0.24	35	SS	3	41.78	-3.36	15	Pli	85/284	03/194	03/104	0.05	14	E	2
41.16	-0.85	11	PUM	76/151	12/333	05/241	0.06	151	E	4	41.70	-3.40	6	PUM	73/017	16/198	01/107	0.19	16	E	1
41.16	-0.85	25	PUM	85/142	03/232	03/322	0.08	55	E	3	41.51	-3.70	12	M	55/347	34/147	03/237	0.64	150	E	2
41.58	-3.22	40	PUM	03/142	85/322	02/232	0.87	142	SS	3	41.51	-3.70	10	M	55/335	34/147	03/245	0.64	151	E	2
42.63	-3.46	20	PUM	87/299	00/209	01/119	0.13	29	E	2	39.95	-6.51	17	M	25/145	64/325	04/055	0.63	144	SS	2
42.63	-3.46	17	PUM	00/061	86/152	03/331	0.76	62	SS	2	39.76	-6.44	10	M	83/068	01/158	06/249	0.15	160	E	1
41.63	-3.39	20	PUM	01/154	82/244	03/064	0.30	155	SS	3	42.83	-3.34	10	PUM	60/297	28/117	03/027	0.08	113	E	1
41.51	-3.30	15	PUM	59/154	29/338	06/244	0.69	154	E	2	42.86	-3.33	41	PUM	88/173	00/353	01/262	0.55	172	E	2
41.51	-3.30	17	PUM	64/194	25/012	00/102	0.68	13	E	2	42.77	-3.01	9	M	18/065	71/245	00/335	0.65	66	SS	2
41.54	-2.95	18	Q	48/050	36/229	17/320	0.30	70	E	2	42.65	-2.98	42	PUM	87/002	00/094	02/184	0.02	95	E	3
41.60	-2.44	6	PUM	13/231	76/054	04/322	0.55	53	SS	1	42.66	-2.13	14	PUM	80/140	06/230	07/321	0.12	57	E	2
41.45	-2.70	12	Q	88/285	01/106	00/016	0.05	106	E	2	42.35	1.74	14	Q	11/168	61/258	26/077	0.09	168	SS	2
41.46	-2.80	10	M	00/319	72/049	17/229	0.04	139	SS	2	42.37	1.72	15	Q	17/007	02/098	72/196	0.45	7	C	2
41.50	-2.36	6	PUM	86/237	02/055	02/146	0.45	56	E	2	42.20	2.77	10	Q	23/190	63/011	11/281	0.64	14	SS	1
41.35	-2.47	10	Q	81/338	02/248	07/157	0.05	59	E	2	42.19	2.80	14	Q	85/274	04/085	00/175	0.02	87	E	2
41.29	-2.23	24	PUM	85/359	04/186	01/096	0.09	6	E	2	42.22	2.67	7	Q	12/052	03/322	77/232	0.52	54	C	1
41.24	-1.93	5	Q	79/195	07/284	07/015	0.17	110	E	1	42.17	2.74	12	Q	86/172	02/262	02/352	0.13	84	E	4
41.25	-3.71	18	M	83/228	01/135	05/045	0.17	135	E	2	42.21	2.78	6	Q	84/177	05/357	05/267	0.08	175	E	2
41.06	-4.41	21	M	06/149	07/240	80/059	0.13	149	C	2	41.97	0.61	24	Q	13/027	03/296	75/206	0.39	28	C	2
41.12	-4.01	17	M	79/335	08/152	04/243	0.03	160	E	3	39.52	-6.67	18	M	75/194	11/284	07/015	0.06	104	E	1
41.14	-4.00	16	M	11/143	24/048	63/236	0.11	144	C	3	39.21	-7.00	18	M	78/345	06/075	09/166	0.08	70	E	2
41.14	-3.88	7	M	22/139	30/035	50/231	0.07	141	C	1	39.29	-5.10	15	Q	64/342	23/159	07/249	0.51	175	SS	2
40.96	-3.21	20	M	04/136	62/037	26/229	0.07	137	SS	2	39.17	-6.98	16	M	22/176	66/356	04/266	0.57	178	SS	1
40.79	-3.67	12	M	33/156	28/046	43/246	0.08	159	C	2	38.99	-6.11	12	Q	34/272	53/90	10/002	0.55	97	SS	2
40.83	-3.57	19	Q	01/314	82/224	07/044	0.55	134	SS	2	38.58	-4.70	37	M	62/151	22/061	14/331	0.42	49	E	2
40.58	-4.73	6	PUM	07/356	59/085	29/265	0.30	175	SS	1	38.53	-4.11	23	PUM	79/142	08/323	04/232	0.30	141	E	2

Table 1. (continued)

Lat,deg	Lon,deg	*N*	DA	σ_1	σ_2	σ_3	*R*	S_{Hmax}	T	*Q*	Lat,deg	Lon,deg	*N*	DA	σ_1	σ_2	σ_3	*R*	S_{Hmax}	T	*Q*
40.09	-6.67	6	M	83/272	06/096	02/006	0.33	96	E	1	38.66	-4.11	18	PUM	87/036	01/306	02/216	0.56	127	E	2
40.05	-6.42	6	M	83/118	06/296	00/026	0.74	117	E	1	38.22	-3.60	14	M	70/154	13/064	13/334	0.05	60	E	2
40.00	-6.10	6	PUM	86/181	03/000	00/090	0.20	1	E	1	38.22	-3.60	10	M	01/000	69/270	20/090	0.73	1	SS	2
40.01	-6.10	18	M	32/132	47/320	24/229	0.16	135	SS	2	41.82	0.78	9	Q	08/008	28/098	59/278	0.23	7	C	2
40.02	-6.10	10	M	80/282	09/096	02/187	0.30	98	E	2	41.80	1.80	9	Q	13/128	44/038	42/238	0.32	131	SS	1

Lat, latitude (north); Lon, longitude (Greenwich meridian); *N*, number of faults; DA, deformation age (M, Miocene; UM = upper Miocene; PUM, post upper Miocene; Pli, Pliocene; Q, Quaternary). Values σ1, σ2, and σ3 are the orientation of the principal axes (dip / dip direction). $R = (\sigma_2 - \sigma_3) / (\sigma_1 - \sigma_3)$. S_{Hmax} is the maximum horizontal stress direction. T is the stress regimen (E, extensional; C, compressional; SS, strike slip). *Q* is the data quality from 5 (high quality) to 0 (low quality).

$$Q = \left(\frac{7}{\alpha}\right)\left(\frac{t}{t+n}\right)\left(1-\frac{4}{t}\right),$$

where α stands for the average angle between theoretical and calculated fault striae, t represents the number of explained faults by the calculated stress tensor, and n is the number of faults unexplained by any tensor [*Herraiz et al.*, 1998]. *Q* values rank from 0 (lowest quality) which corresponds to $Q=0$, to 4 (highest quality), which corresponds to $Q \geq 0.7$. Intermediate values are 1 for $0 < Q < 0.1$, 2 for $0.1 \leq Q < 0.4$, and 3 for $0.4 \leq Q < 0.7$. As it can be noticed, this parameter considers criteria similar to those adopted by *Rebaï et al.* [1992], and it is easy to establish an equivalence of qualities 1-4 from both classifications. The relationship with the *Zoback's* [1992] criteria is not as easy, but the results rated with 4, 3, and 2 indicate very good to fairly good in quality and can be assimilated to qualities A and B from Zoback's classification. Quality 1 represents poor quality, and 0 indicates that the corresponding result has been discarded.

The seismological information compiled to estimate the present stress state consisted of 156 earthquakes located on the Iberian Peninsula and surrounding areas and selected from the data file of the Instituto Geográfico Nacional (IGN) for the period January 1, 1980, to December 31, 1995. The reason for having chosen this starting date was that from that time on the Spanish Seismic Network has fulfilled the necessary quality requirements.

The selection from the data file was accomplished in different steps. The first choice was a sample of 1981 earthquakes with magnitudes greater than or equal to 3.0 and focal depths less than or equal to 30 km. Their corresponding hypocenters had been calculated with a number of observations greater than or equal to 7 and solutions having the root-mean-square travel time residual (RMS) less than or equal to 1 s and the vertical and horizontal errors (ERZ and ERH, respectively) less than or equal to 5 km. This initial set was carefully analyzed in such a way that all the phases were read again and the first arrival *P* wave polarities were checked. The hypocenters were recalculated using the HYPOINVERSE program [*Klein*, 1978] and the crustal model adopted by the IGN for the whole Iberian Peninsula [*Mezcua and Rueda*, 1993]. This process required reading 10728 *P* phases and 8566 *S* phases. A new selection was made keeping the conditions already mentioned for RMS, ERZ, ERH, and focal depth and choosing only the events with at least 7 polarities, 10 observations (first *P* and/or *S* arrival time readings), 1 *S* phase with weight greater than or equal to 0.1, and condition number lower than 100. No maximum gap selection criterion was used. The new data bank of 128 earthquakes included 3 events with magnitude lower than 3.0 that had occurred in an interesting area from the tectonic point of view (Guadalquivir Basin) and from which very precise information obtained with a local microseismic survey was available [*Herraiz et al.*, 1996]. This sample was increased with the other 28 events chosen from the bibliography because of their magnitude, location, and accuracy [*Vidal*, 1986; *Delouis et al.*, 1993; *Buforn et al.*, 1995; *Goula et al.*, 1999]. The polarities of the earthquakes that occurred in Catalonia and the eastern Pyrenees were obtained from the data file of the Institut Cartogràfic de Catalunya. Three of the added events, Lorca (June 6, 1977, $M = 4.2$), Alcocer (June 30, 1979, $M = 4.1$), and the Pyrenees (February 12, 1996, $M = 5.3$), took place out of the 1980-1995 period but were considered in the series because of their location and magnitude.

The total sample (156 events) includes 2372 *P* wave polarities (*Pn* or *Pg* phases). The histograms of the magnitudes and the number of polarities corresponding to these earthquakes are plotted in Figure 1. Finally, five more events with five or six polarities have been added to the last set only when the technique developed by *Giner* [1996] was applied. The main focal parameters of the 161 events are listed in Table 3.

3. Methodology

3.1. Recent Stress Tensor

Three techniques of fault population analysis were successively applied: the slip model [*Reches*, 1983; *De Vicente*, 1988], the right dihedra method [*Angelier and Mechler*, 1977], and the stress inversion method [*Carey and Brunier*, 1974; *Carey*, 1979; *Reches*, 1987; *Reches et al.*, 1992]. The slip model was used to establish fault groups compatible with the same horizontal shortening direction. This model was applied after checking that the main assumptions concerning the data taken in the field were satisfied [*Capote et al.*, 1991] and that their angular errors were lower than 5°. When a generalized data misfit was observed, attention was paid to check the presence of later tilting or folding. In these cases, and when it was possible to do so, the structures were restored to their original position.

The right dihedra method was applied to both the whole data set of each station and the subpopulations obtained through the slip model. Next, the stress inversion method [*Reches et al.*, 1992] was applied to the whole population to establish, if possible, several fracturation episodes. These results were compared to those obtained previously, and if similar, the fault groups made in the first step were considered correct. In every

Table 2. Maximum Horizontal Shortening Directions Taken From Bibliographical Information

Lat,deg	Lon,deg	Def Age	S_{Hmax}	Ref	Lat,deg	Lon,deg	Def Age	S_{Hmax}	Ref	Lat,deg	Lon,deg	Def Age	S_{Hmax}	Ref
37.37	-2.98	M	26	1	36.92	-3.66	M	136	1	38.75	-0.02	UM	141	2
37.37	-2.98	M	139	1	37.09	-3.53	M	124	1	38.63	-0.01	UM	172	2
37.32	-3.56	M	8	1	37.09	-3.53	M	112	1	38.73	-0.35	UM	18	2
37.32	-3.56	M	176	1	37.21	-3.47	M	40	1	38.56	-0.48	UM	139	2
37.32	-3.56	M	164	1	37.21	-3.47	M	152	1	38.53	-0.53	UM	132	2
37.37	-3.73	M	47	1	37.25	-3.38	M	74	1	38.72	-0.46	UM	38	2
37.37	-3.73	M	34	1	37.25	-3.38	M	137	1	38.52	-0.40	UM	32	2
37.37	-3.73	M	120	1	37.29	-3.30	M	97	1	36.87	-5.97	Q	130	3
37.41	-3.66	M	62	1	37.17	-3.53	M	4	1	36.71	-6.12	Q	135	3
37.41	-3.66	M	90	1	36.27	-5.50	Q	150	3	36.71	-5.85	Q	155	3
37.43	-3.66	M	176	1	36.74	-5.02	Q	160	3	36.49	-6.18	Q	177	3
37.43	-3.66	M	126	1	36.21	-5.49	Q	10	3	36.29	-6.15	Q	160	3
37.51	-3.72	M	20	1	36.23	-5.48	Q	170	3	36.18	-5.99	Q	145	3
37.51	-3.72	M	53	1	36.28	-5.48	Q	162	3	37.11	-4.98	Q	173	3
37.58	-3.69	M	144	1	37.11	-2.11	Q	27	4	36.60	-6.26	Q	62	3
37.58	-3.69	M	113	1	37.11	-2.08	Q	156	4	36.31	-6.21	Q	3	3
37.58	-3.69	M	12	1	37.11	-2.01	Q	104	4	36.19	-6.01	Q	155	3
37.59	-3.65	M	171	1	37.09	-2.06	Q	153	4	36.10	-5.73	Q	165	3
37.59	-3.65	M	139	1	37.09	-2.01	Q	102	4	37.33	-3.67	Q	0	5
37.61	-3.85	M	94	1	37.07	-2.06	Q	11	4	37.22	-4.15	Q	160	5
37.61	-3.85	M	119	1	37.08	-2.04	Q	154	4	37.23	-3.90	Q	170	5
37.66	-3.67	M	34	1	37.08	-2.02	Q	114	4	37.19	-3.80	Q	80	5
37.66	-3.67	M	130	1	37.05	-2.04	Q	60	4	37.06	-3.88	Q	160	5
37.78	-3.84	M	42	1	37.04	-2.09	Q	103	4	37.14	-3.41	M	169	1
37.78	-3.84	M	54	1	37.05	-2.08	Q	6	4	37.14	-3.41	M	105	1
38.04	-2.89	M	152	1	37.03	-2.08	Q	107	4	37.06	-3.47	M	172	1
38.04	-2.89	M	98	1	37.04	-2.05	Q	130	4	37.06	-3.47	M	69	1
38.09	-2.84	M	23	1	37.04	-1.97	Q	108	4	37.02	-3.49	M	120	1
38.09	-2.84	M	140	1	37.11	-2.08	UM	179	4	37.02	-3.49	M	135	1
38.17	-2.81	M	141	1	37.11	-2.09	UM	178	4	36.92	-3.45	M	72	1
38.17	-2.81	M	129	1	37.10	-2.07	UM	175	4	36.92	-3.45	M	0	1
38.54	-0.48	MM-UM	141	2	37.09	-2.01	UM	164	4	36.95	-3.26	M	86	1
38.55	-0.50	MM-UM	129	2	37.07	-2.07	UM	161	4	36.95	-3.26	M	84	1
38.33	-0.69	MM-UM	134	2	37.08	-2.04	UM	171	4	36.92	-3.66	M	106	1
38.59	-0.78	MM-UM	138	2	37.05	-2.05	UM	154	4	36.85	-2.00	Q	165	6
38.56	-0.48	MM-UM	42	2	37.06	-2.04	UM	161	4	36.85	-1.98	Q	170	6
38.56	-0.26	MM-UM	131	2	37.07	-2.02	UM	160	4	37.16	-3.47	Q	175	5
38.54	-0.51	MM-UM	114	2	37.05	-2.08	UM	170	4	37.06	-3.46	Q	160	5
38.52	-0.40	MM-UM	80	2	37.04	-2.06	UM	178	4	42.52	-3.89	UM	95	7
38.52	-0.50	MM-UM	103	2	37.05	-2.07	UM	162	4	42.57	-3.90	UM	105	7
38.53	-0.53	MM-UM	107	2	37.12	-2.01	UM	119	4	42.54	-3.79	UM	80	7
38.58	-0.26	MM-UM	94	2	37.12	-1.98	UM	129	4	42.46	-3.83	UM	142	7
39.11	-0.68	UM	111	2	37.11	-2.01	UM	111	4	42.41	-3.61	UM	85	7
38.99	-0.18	UM	154	2	37.08	-2.06	UM	139	4	41.67	-3.02	Q	175	8
38.77	0.06	UM	117	2	37.09	-2.00	UM	123	4	41.54	-2.77	MM	25	8
38.71	-0.04	UM	155	2	37.09	-2.01	UM	137	4	41.60	-2.44	UM	175	8
41.53	-2.26	Pli	50	8	41.95	-0.27	M	165	11	41.64	2.34	Q	60	15
41.46	-2.61	UM	45	8	41.88	-0.20	M	124	11	41.45	1.62	Q	45	15
41.46	-2.68	UM	70	8	41.97	-0.51	M	107	11	42.06	-1.15	MM	150	9
37.05	-2.08	UM	128	4	41.42	-2.79	UM	40	8	41.97	-0.48	M	139	11
37.05	-2.05	UM	127	4	41.37	-2.71	Pli	20	8	41.96	-0.41	M	145	11
37.05	-2.05	UM	121	4	41.36	-2.47	Pli	24	12	41.85	-0.28	M	139	11
37.05	-2.03	UM	145	4	41.28	-2.44	Pli	64	10	41.79	-0.46	M	20	11
37.06	-2.02	UM	149	4	41.24	-2.29	Pli	30	12	41.83	-0.39	M	22	11
37.07	-2.02	UM	133	4	41.24	-2.29	Pli	4	12	41.82	-0.24	M	21	11
37.06	-2.01	UM	141	4	41.25	-1.94	Pli	140	8	41.73	-0.25	M	40	11
37.05	-2.00	UM	127	4	42.12	-1.76	UM	5	13	41.69	-0.21	M	167	11
37.05	-1.99	UM	141	4	42.12	-1.76	UM	55	13	41.78	-0.36	M	98	11
37.03	-2.08	UM	145	4	40.96	-0.45	UM	15	8	41.77	-0.36	M	119	11
37.03	-2.06	UM	128	4	41.45	-1.11	UM	44	11	41.74	-0.44	M	108	11
37.03	-1.99	UM	125	4	41.56	-0.21	UM	26	11	41.71	-0.28	M	101	11
37.04	-1.97	UM	130	4	41.63	-0.33	UM	7	11	41.69	-0.27	M	92	11
37.02	-1.85	UM	113	6	41.52	-0.51	UM	122	11	41.69	-0.23	M	103	11
37.00	-1.86	UM	125	6	41.25	-0.90	LM	46	11	41.67	0.09	M	0	11
37.00	-1.92	UM	145	6	41.22	-0.93	LM	134	11	41.71	-0.03	M	102	11
36.90	-2.00	UM	140	6	41.26	-0.96	LM	130	11	41.70	0.10	M	95	11
36.89	-1.97	UM	125	6	41.25	-0.93	LM	141	11	41.72	0.12	M	74	11

Table 2. (continued)

Lat,deg	Lon,deg	Def Age	$S_{H\max}$	Ref	Lat,deg	Lon,deg	Def Age	$S_{H\max}$	Ref	Lat,deg	Lon,deg	Def Age	$S_{H\max}$	Ref
36.88	-1.94	UM	155	6	41.21	-0.99	LM	41	11	41.81	-0.03	M	128	11
36.89	-1.94	UM	155	6	41.53	-0.93	MM	124	11	41.77	-0.06	M	101	11
36.90	-1.93	UM	130	6	41.63	-0.98	MM	83	11	41.76	-0.04	M	104	11
36.88	-1.92	UM	140	6	41.50	-0.30	UM	149	11	41.75	-0.17	M	123	11
36.90	-1.87	UM	153	6	41.35	-0.35	UM	146	11	41.82	-0.16	M	120	11
37.02	-1.85	Q	170	6	41.83	-0.52	UM	128	11	41.80	-0.14	M	126	11
37.02	-1.84	Q	167	6	41.82	-0.53	UM	87	11	41.79	-0.06	M	136	11
37.01	-1.95	Q	164	6	41.40	-0.75	LM	141	11	41.55	-0.37	M	111	11
37.00	-1.86	Q	170	6	41.46	-0.80	LM	146	11	41.58	-0.22	M	128	11
36.89	-1.89	Q	3	6	41.58	-1.17	UM	61	11	41.62	-0.21	M	108	11
36.89	-1.91	Q	179	6	41.55	-0.08	UM	138	11	41.65	-0.21	M	48	11
36.89	-1.93	Q	170	6	41.56	-0.08	UM	139	11	41.61	-0.25	M	115	11
36.89	-1.93	Q	170	6	41.92	-0.93	UM	96	11	41.55	0.12	M	125	11
36.89	-1.95	Q	168	6	41.97	-0.96	UM	102	11	41.49	-1.15	M	83	11
36.89	-1.96	Q	175	6	41.60	-1.09	UM	151	11	41.43	-0.39	M	140	11
36.90	-1.97	Q	178	6	41.60	-1.09	UM	143	11	41.37	-0.50	M	131	11
40.11	-0.53	UM	175	9	41.60	-1.09	UM	158	11	41.37	-0.43	M	116	11
41.94	-0.71	UM	135	8	41.60	-1.09	UM	144	11	41.27	0.14	M	123	11
40.08	-0.56	UM	67	10	41.60	-1.09	UM	100	11	41.85	-2.04	Pli	25	14
40.05	-1.53	UM	180	8	41.85	-1.86	Q	140	14	41.84	-1.98	M	45	14
39.34	-1.39	Pli	10	10	40.74	0.49	Q	135	15	41.66	-2.04	Pli	25	14
42.12	-0.80	M	139	11	40.81	0.52	Q	145	15	42.54	2.72	Q	50	16
42.11	-0.71	M	130	11	41.03	0.56	Q	170	15	42.81	2.85	Q	160	16
42.13	-0.76	M	112	11	41.40	1.98	Q	130	15	42.85	3.05	Q	180	16
41.95	-0.22	M	176	11	40.96	0.80	Q	90	15	42.72	1.88	Q	170	16
41.91	-0.22	M	129	11	41.05	0.85	Q	180	15	43.56	-1.98	Pli	90	14
41.91	-0.26	M	134	11	41.09	0.92	Q	125	15	42.61	-2.24	Pli	80	14
41.92	-0.27	M	117	11	41.23	1.12	Q	40	15	42.61	-1.62	Pli	40	14
42.72	-2.28	Q	85	17	40.27	-1.22	UM	7	10	42.26	-0.55	M	180	11
41.97	-8.65	Q	118	18	40.27	-1.22	UM	32	10	42.25	-0.13	M	2	11
37.69	-8.57	Q	19	18	40.27	-1.19	UM	39	10	42.04	-0.56	M	3	11
37.52	-8.69	Q	11	18	40.27	-1.19	UM	170	10	41.66	-0.37	M	10	11
37.35	-8.83	Q	5	18	40.27	-1.19	UM	104	10	41.56	-0.21	M	4	11
39.83	-7.35	Q	149	18	40.18	-0.83	UM	145	14	41.66	-0.24	M	2	11
38.17	-7.65	Q	147	18	40.17	-0.55	UM	125	14	42.02	-0.98	M	3	11
38.17	-7.75	Q	173	18	41.23	0.30	M	180	11	42.02	-0.94	M	10	11
41.27	-7.07	Q	170	18	41.27	0.33	M	166	11	41.49	0.45	M	5	11
40.31	-7.86	Q	140	18	41.30	0.38	M	14	11	41.45	0.20	M	13	11
38.07	-8.75	Q	120	18	41.65	0.16	M	7	11	41.65	0.13	M	172	11
40.99	-1.10	M	10	19	41.57	0.38	M	171	11	41.67	0.05	M	177	11
40.66	-1.37	Pli	33	10	41.62	0.40	M	3	11	41.59	-0.05	M	20	11
40.66	-1.37	Pli	1	10	41.38	-0.43	M	7	11	41.92	-1.02	M	4	11
40.66	-1.37	Pli	146	10	41.38	-0.21	M	0	11	41.69	-0.00	M	172	11
40.66	-1.37	Pli	22	10	41.83	-0.52	M	0	11	41.68	0.06	M	11	11
40.45	-1.25	UM	122	20	41.70	-0.35	M	4	11	41.98	-0.65	M	174	11
40.44	-1.13	Q	130	8	41.75	-0.41	M	166	11	41.94	-0.59	M	0	11
40.24	-1.13	MM	69	9	41.83	-0.53	M	1	11	41.85	-0.53	M	3	11
40.39	-1.23	Pli	33	10										

Lat, latitude (north); Lon, longitude (Greenwich meridian); Def Age, deformation age (M, Miocene; LM, lower Miocene; MM, middle Miocene; UM, upper Miocene; Pli, Pliocene; Q, Quaternary). $S_{H\max}$ is the maximum horizontal stress direction. Ref, reference (1, *Galindo-Zaldívar et al.* [1993]; 2, *De Ruig* [1992]; 3, *Benkhelil* [1976]; 4, *Stapel et al.* [1996]; 5, *Sanz de Galdeano* [1985]; 6, *Huibregtse et al.* [1998]; 7, J.L. Simón (unpublished data, 1990a); 8, *Cortés and Maestro* [1997]; 9, *Paricio and Simón* [1986]; 10, Simón [1989]; 11, *Arlegui* [1996]; 12, *Maestro* [1994]; 13, *Casas* [1990]; 14, Cortés *and Simón* [1997]; 15, *Massana* [1995]; 16, *Goula et al.* [1996]; 17, J.L. Simón (unpublished data, 1990a); 18, *Ribeiro et al.* [1996]; 19, *Colomer* [1987]; 20, *Simón and Soriano* [1993].

case the angular confidence margins of the main stress axes have been estimated using the bootstrapping technique [*Stuart*, 1984]. The three methods used in the fault analysis (slip model, right dihedra, and *Reches et al.*'s [1992] method) show analogous results although the last one gives the most complete solution. Then, in order to simplify the presentation of the fault data results, only those obtained with Reches et al.'s method have been shown. More detailed information can be found in the work of *Herraiz et al.* [1998].

Fault population analysis provided 824 orientations of the maximum horizontal stress $S_{H\max}$, from which 474 were obtained from field data and 350 were obtained from bibliographical information. $S_{H\max}$ trends and geologic site locations are plotted in Figure 2. Histograms of these orientations and the stress tensors deduced for each trend appear in Figure 3. In some sites the analytical procedure has yielded two or more stress tensors, but their chronological sequence has been established only in a few cases.

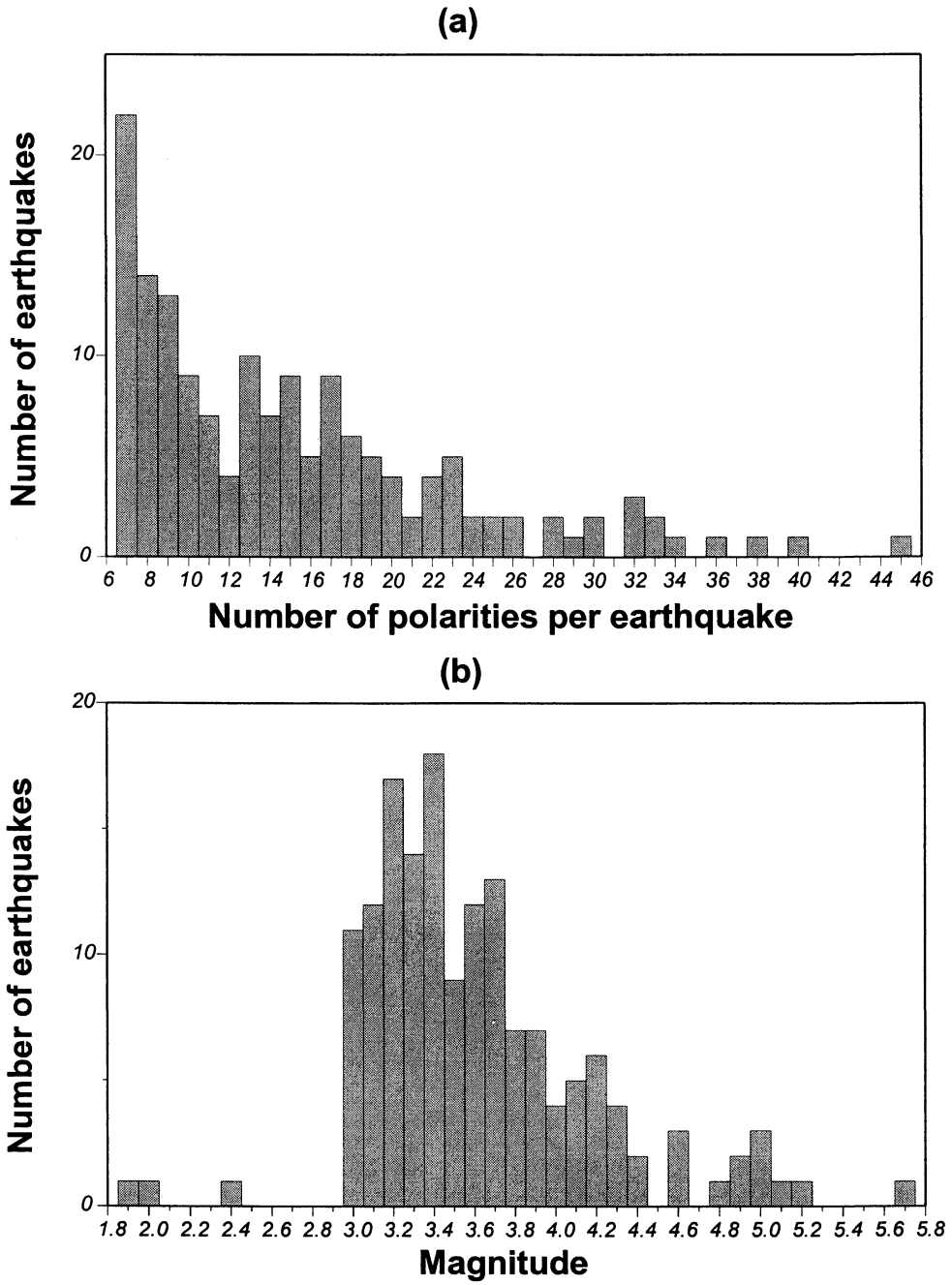

Figure 1. (a) Histogram of number of polarities per earthquake used in the simultaneous inversion of the stress tensor and the individual focal mechanisms [*Rivera and Cisternas*, 1990] considering the main database (156 events; see also Table 3). (b) Histogram of the earthquake magnitudes for the same set of earthquakes.

3.2. Present-Day Stress Tensor

The study of the present-day stress field has been made using two different procedures. The first one was the application of *Rivera and Cisternas*'s [1990] method to obtain the stress tensor inversion using the data set of 156 earthquakes and 2372 P wave polarities described in section 2. This method assumes *Bott*'s [1959] hypothesis and the homogeneity of the stress field in the region of interest. The main feature is that polarities are the input data instead of previously calculated fault plane solutions. The algorithm seeks the maximum of a likelihood function that depends on the radiation pattern function and on the probability of obtaining either a compressive or a dilatational polarity. The algorithm calculates the shape and orientation of the stress tensor in the studied area and the individual fault plane solutions consistent with it. The shape of the tensor is usually given by the stress ratio R, defined as $R = (\sigma_2 - \sigma_3)/(\sigma_1 - \sigma_3)$, where σ_1, σ_2, and σ_3 are the maximum, the intermediate, and the minimum

Table 3. Hypocentral Parameters of the Earthquakes Chosen to Study the Present Stress State

Event	Date	Hour	Minute	Second	Lat,deg	Lon,deg	Depth, km	RMS, s	*Erh*, km	*Erz*, km	*M*	N Polarities
						External Betics						
1	March 5, 1981	1	21	52	38.49	0.21	1	1.0	3	4	4.9	38
2	Sept. 14, 1985	4	25	1	37.38	-3.65	7	0.6	2	2	3.5	16
3	April 26, 1986	0	12	1	37.22	-3.72	5	0.6	1	1	4.0	21
4	May 30, 1985	11	22	26	37.09	-4.26	5	0.8	2	2	3.7	15
5	July 5, 1986	16	35	5	38.77	-0.24	11	0.5	2	2	3.4	7
6	March 11, 1987	0	36	41	37.73	-3.40	6	0.9	2	2	4.3	29
7	June 7, 1989	0	12	48	37.15	-4.53	6	0.3	1	1	3.4	15
8	March 29, 1990	3	10	21	38.29	0.16	8	0.6	1	2	3.6	8
9	Aug. 14, 1991	10	32	9	38.75	-0.96	4	0.9	1	2	4.1	19
10	Aug. 20, 1992	3	38	56	38.26	-0.88	16	0.5	1	2	3.0	8
11	Nov. 11, 1993	2	5	60	38.31	-0.91	4	0.7	1	2	3.2	8
12	Nov. 11, 1993	7	33	24	38.18	0.00	8	0.7	1	1	3.7	23
13	Dec. 5, 1993	14	15	42	38.48	-1.26	3	0.7	1	2	3.2	15
14	Dec. 11, 1993	2	51	9	38.05	-0.65	9	0.3	1	1	3.4	8
15	Jan. 20, 1994	6	32	40	37.26	-4.23	6	0.9	1	2	3.3	15
16	March 5, 1994	15	26	7	36.96	-4.37	7	0.4	1	1	3.2	17
17	March 23, 1994	15	10	31	37.83	-4.14	8	0.6	1	1	3.4	17
18	June 7, 1994	3	10	36	38.9	-0.39	16	0.5	1	1	3.0	8
19	Aug. 4, 1994	6	43	42	38.18	-1.06	3	0.7	1	2	3.3	9
20	Aug. 10, 1994	20	5	16	37.20	-4.35	2	0.9	1	2	3.1	15
21	Sept. 6, 1994	2	0	30	36.81	-5.40	6	0.8	1	1	3.7	22
22	Sept. 23, 1994	15	41	25	37.07	-4.32	5	0.6	1	1	3.1	13
23	Oct.7, 1994	12	51	17	36.23	-6.10	17	0.6	1	1	3.0	12
24	Nov. 28, 1994	7	30	21	38.51	-1.25	8	0.7	1	2	3.4	12
25	Jan. 25, 1995	20	13	11	37.85	-4.07	5	0.6	1	1	3.2	16
26	June 6, 1995	14	58	50	37.25	-4.19	2	0.6	1	3	3.1	7
27	July 1, 1995	3	29	8	37.45	-3.80	14	0.7	1	2	3.4	7
28	July 11, 1995	18	27	34	37.45	-3.82	20	0.5	1	1	3.6	11
29	Oct. 4, 1995	2	6	7	38.80	0.32	6	0.6	1	2	3.8	13
30	Nov. 26, 1995	5	39	40	38.00	-1.23	2	0.6	1	1	4.1	18
31	Nov. 26, 1995	6	25	6	38.02	-1.26	1	0.7	1	2	3.7	11
32	Dec. 6, 1995	10	13	31	38.00	-1.27	7	0.6	1	1	3.6	7
33	Dec. 18, 1995	3	47	15	37.46	-3.76	24	0.5	1	1	3.3	10
						Internal Betics						
34	June 6, 1977	10	49	12	37.65	-1.73	9	0.8	3	11	4.2	22
35	June 24, 1984	14	30	51	36.84	-3.74	5	0.7	2	2	5.0	45
36	Sept. 13, 1984	4	34	11	36.98	-2.34	9	0.9	4	4	5.0	28
37	Sept. 16, 1985	22	25	9	37.02	-3.82	5	0.6	2	2	3.0	11
38	Aug. 16, 1986	18	10	40	37.07	-3.22	9	0.3	1	1	3.0	9
39	March 20, 1988	19	44	47	37.14	-2.10	1	0.3	1	1	3.1	7
40	May 2, 1988	10	51	17	37.18	-3.61	11	0.2	1	1	3.0	8
41	Aug. 20, 1988	16	42	52	37.19	-3.74	2	0.4	1	1	3.4	13
42	Dec. 6, 1988	6	9	16	37.03	-3.85	4	0.4	1	1	3.1	14
43	Dec. 22, 1993	20	11	38	37.01	-3.94	1	0.8	1	2	3.6	23
44	Dec 23, 1993	18	0	8	36.75	-2.99	2	0.9	1	1	3.8	26
45	Jan. 3, 1994	1	0	7	36.79	-2.97	7	0.6	1	1	3.7	32
46	Jan. 4, 1994	8	3	15	36.56	-2.83	6	0.6	1	2	4.9	34
47	Jan. 4, 1994	8	47	28	36.60	-2.84	9	0.5	1	1	3.5	17
48	Jan. 8, 1994	22	48	8	37.07	-3.91	2	0.5	1	1	3.6	28
49	Jan. 9, 1994	16	1	36	36.61	-2.86	13	0.3	2	1	3.1	17
50	Jan. 16, 1994	15	55	4	36.56	-2.86	6	0.8	1	1	3.4	18
51	Jan. 16, 1994	17	3	10	36.64	-2.85	5	0.9	1	2	3.5	15
52	Jan. 17, 1994	5	50	27	37.28	-3.16	7	0.3	1	1	3.2	19
53	Jan. 26, 1994	16	16	45	36.65	-2.83	3	0.6	1	2	3.7	23
54	Feb. 2, 1994	6	3	6	36.67	-2.81	10	0.6	1	1	3.4	21
55	Feb. 2, 1994	18	3	40	36.49	-2.80	11	0.7	1	2	3.7	33
56	March 11, 1994	21	42	38	37.33	-1.81	4	0.8	1	1	3.2	18
57	March 29, 1994	14	29	2	36.62	-2.80	6	0.8	1	1	3.5	14
58	March 29, 1994	22	4	21	36.67	-3.36	4	0.7	1	1	3.7	33
59	March 30, 1994	23	26	44	37.06	-2.51	3	0.5	1	1	3.1	22
60	April 8, 1994	4	0	5	37.37	-2.01	2	0.6	1	1	3.9	40
61	April 8, 1994	4	13	33	37.35	-2.04	2	0.6	1	1	3.1	15
62	April 19, 1994	23	52	0	37.34	-2.00	7	0.5	1	1	3.7	26
63	April 20, 1994	21	23	38	37.35	-2.04	1	0.5	1	1	3.2	13
64	April 23, 1994	17	53	59	37.36	-2.02	2	0.6	1	1	3.2	17
65	June 12, 1994	6	31	46	36.93	-2.04	5	0.5	1	1	3.1	13
66	July 13, 1994	10	12	31	36.52	-3.82	2	0.6	1	2	3.3	18
67	July 24, 1994	0	45	22	36.99	-2.51	11	0.4	1	1	3.3	24
68	Nov. 8, 1994	0	17	35	36.98	-2.35	3	0.9	1	2	4.0	36

Table 3. (continued)

Event	Date	Hour	Minute	Second	Lat,deg	Lon,deg	Depth, km	RMS, s	*Erh*, km	*Erz*, km	*M*	N Polarities
						Internal Betics (continued)						
69	Dec. 3, 1994	18	42	44	37.29	-2.98	9	0.5	1	1	3.5	20
70	Dec. 25 1994	12	4	28	36.07	-3.09	1	0.8	1	2	3.3	10
71	Feb. 25, 1995	19	24	25	37.31	-2.64	2	0.5	1	2	3.2	17
72	March 17, 1995	14	4	14	37.16	-3.79	6	0.6	1	1	3.9	19
73	March 18, 1995	13	40	34	37.09	-2.16	1	0.4	1	1	3.9	30
74	April 29, 1995	7	37	41	36.73	-2.83	6	0.7	1	2	3.1	14
75	May 18, 1995	23	13	6	36.85	-3.00	1	0.4	1	3	3.1	9
76	May 29, 1995	16	21	27	36.87	-3.86	6	0.6	1	1	3.0	11
77	June 7, 1995	16	20	36	36.92	-2.17	8	0.6	1	1	4.0	17
78	Sept. 18, 1995	5	14	41	36.94	-4.07	1	0.5	1	2	3.0	7
79	Nov. 9, 1995	19	20	53	36.40	-2.72	6	0.6	1	2	3.4	7
80	Nov. 18, 1995	0	24	48	36.97	-2.53	3	0.3	1	1	4.0	18
						Guadalquivir Basin						
81	Aug. 13, 1994	16	25	18	36.46	-7.24	25	0.5	1	2	3.5	23
82	Aug. 28, 1994	13	43	12	36.72	-7.79	24	0.9	2	2	3.3	20
83	Sept. 26, 1994	20	2	17	36.76	-7.77	27	0.6	2	1	3.0	10
84	Dec. 26, 1994	17	48	22	36.49	-7.79	28	0.7	1	2	3.6	9
85	March 5, 1995	23	46	23	36.10	-7.48	14	0.7	2	2	3.7	25
						Iberian Range						
86	May 14, 1986	23	55	37	39.90	-1.40	9	0.8	2	2	3.3	19
87	Oct. 28, 1986	6	48	10	39.84	-1.30	5	0.5	2	3	3.2	9
88	July 6, 1987	4	32	25	40.95	-1.00	5	0.6	2	3	3.4	13
89	Aug. 24, 1987	18	43		40.93	1.57	8				4.2	10
90	May 19, 1988	21	16	31	39.54	-1.04	2	0.5	2	2	3.2	13
91	Dec. 28, 1988	6	21	15	39.40	-0.29	17	0.6	1	2	3.4	7
92	Sept. 24, 1989	20	16	4	41.20	-1.15	6	0.8	3	2	3.3	13
93	Dec. 15, 1991	11	50		40.98	2.06	12				4.2	15
94	Dec. 21, 1991	5	8	25	39.42	-0.79	2	0.9	1	2	3.3	7
95*	Jan. 24, 1992	9	49	32	40.86	-2.39	1	0.6	3	3	3.4	6
96	May 25, 1993	7	7	13	39.43	-0.80	2	2.3	1	1	3.3	13
97	Aug. 15, 1993	22	32	25	40.29	-1.09	3	0.5	2	3	3.4	16
98	Oct. 25, 1993	0	16	6	40.59	-1.58	2	0.5	2	2	3.2	11
99	Sept. 26, 1994	5	38		41.41	2.55	10				4.2	9
100	May 15, 1995	15	37		40.80	1.52	15				4.6	14
						Northwest						
101	Dec. 12, 1988	12	14	40	42.16	-7.76	5	0.2	1	1	3.2	7
102	Dec. 30, 1988	16	41	39	42.15	-7.75	3	0.2	1	1	3.2	7
103	June 10, 1989	7	15	8	42.16	-7.78	11	0.3	1	1	3.2	8
104	Aug. 30, 1989	11	43	26	42.11	-7.52	14	0.5	1	1	3.8	10
105	Nov. 22, 1990	4	33	14	42.28	-7.61	17	0.5	1	2	3.6	8
106	April 15, 1994	13	26	19	43.56	-7.36	29	0.7	1	2	4.2	24
107	Nov. 29, 1995	23	56	29	42.83	-7.32	10	0.6	1	3	4.6	25
108	Nov. 30, 1995	2	20	34	42.82	-7.31	10	0.2		2	3.8	17
109	Dec. 24, 1995	15	49	43	42.82	-7.17	16	0.1	1	1	3.7	8
						Pyrenees-Ebro Basin						
110	Feb. 29, 1980	20	41		43.17	-0.39	6				5.7	32
111	July 19, 1981	19	58		43.09	0.07	6				4.6	8
112	Sept. 28, 1981	1	41		43.17	-0.03	13				4.3	10
113	June 22, 1982	19	50	23	42.86	-1.81	1	0.7	2	2	4.4	7
114	Aug. 25, 1982	20	59		43.07	-0.28	8				4.3	10
115	Feb. 25, 1984	2	3	19	43.21	-1.12	11	0.5	1	2	4.8	16
116	Sept. 30, 1985	2	28		43.03	-0.44	6				3.8	7
117	April 19, 1986	9	1		43.09	-0.51	10				3.9	10
118	May 26, 1987	16	32		43.13	-0.38	4				3.8	9
119	June 26, 1987	17	13		43.08	-0.41	3				3.9	9
120	Nov. 7, 1987	11	7	52	43.04	-3.70	16	0.5	2	2	3.9	7
121	Nov. 11, 1987	7	15		43.07	-0.18	8				4.1	8
122	Nov. 12, 1987	1	33	13	43.17	-0.17	1	0.4	1	1	3.6	7
123	Dec. 15, 1987	7	35		43.43	-0.61	11				3.9	11
124	Jan. 6, 1989	19	33		42.99	0.17	11				4.4	16
125	Feb. 28, 1990	13	23	43	42.91	-1.04	10	0.7	2	2	3.6	15
126	April 1, 1990	19	13	34	43.15	-1.43	13	0.4	1	1	3.4	8
127	June 19, 1990	21	48	12	42.79	-1.66	3	0.6	1	1	3.4	10
128	July 26, 1990	16	29	34	42.50	-1.15	1	0.7	2	4	3.6	9
129	Aug. 5, 1990	21	32		42.27	1.09	1				3.7	9
130	March 19, 1992	18	53		42.23	2.06	2				4.2	18

Table 3. (continued)

Event	Date	Hour	Minute	Second	Lat,deg	Lon,deg	Depth, km	RMS, s	*Erh*, km	*Erz*, km	*M*	N Polarities
					Pyrenees-Ebro Basin (continued)							
131	Oct. 8, 1993	22	9		42.43	2.13	3				3.3	13
132	Feb. 18, 1996	1	45		42.80	2.53	8				5.2	22
					Central System							
133	July 7, 1990	23	30	18	40.73	-3.54	4	0.8	2	2	3.3	20
134	Nov. 17, 1995	15	11	48	40.57	-4.00	12	0.4	1	1	3.3	9
					Duero Basin							
135	April 13, 1994	3	33	4	41.55	-3.10	12	0.3	2	11	3.4	11
					Tajo Basin - Mancha Plain							
136	June 30, 1979	1	44	36	40.66	-2.52	10	1.4	8	7	4.1	9
137	Feb. 23, 1982	17	59	15	40.64	-2.75	7	1.3	3	5	4.1	8
138	May 13, 1986	18	38	44	39.23	-2.73	5	0.7	2	3	3.6	19
139	May 13, 1986	20	24	19	39.23	-2.67	5	0.7	4	3	3.0	12
140	Oct. 19, 1987	12	54	43	40.26	-3.24	5	0.4	1	1	3.2	7
141*	Sept. 28, 1988	12	43	51	40.10	-3.54	2	0.3	2	4	3.0	6
142	Oct. 4, 1988	13	5	11	40.08	-3.56	2	0.3	1	3	3.1	8
143*	Oct. 11, 1988	14	15	29	40.07	-3.58	2	0.4	2	3	3.1	6
144	Oct. 24, 1988	4	38	52	40.07	-3.24	9	0.4	2	2	3.4	14
145	Feb. 20, 1989	3	25	37	38.90	-3.09	8	0.5	2	2	3.6	23
146	Nov. 30, 1990	21	52	12	39.21	-2.83	2	0.6	3	2	3.0	7
147	May 30, 1991	20	10	39	39.23	-2.31	4	0.5	1	2	3.5	14
148	April 20, 1992	2	8	26	39.52	-2.54	8	0.4	1	2	3.4	9
149	Feb. 6, 1994	5	27	0	39.50	-3.33	6	0.6	1	6	3.5	7
150*	Feb. 14, 1994	12	3	50	40.45	-2.62	16	0.3	1	2	2.8	5
151*	March 29 1995	16	10	7	39.62	-2.79	1	0.6	1	2	3.1	5
					Toledo - Sierra Morena Mountains							
152	May 26, 1985	18	5	10	37.79	-4.64	5	0.6	2	2	5.1	32
153	May 8, 1986	23	10	37	38.10	-4.40	5	0.7	2	3	3.2	14
154	Dec. 20, 1989	4	15	5	37.27	-7.37	17	0.4	1	2	5.0	20
155	March 10, 1991	11	17	6	37.75	-5.49	15	0.1	2	2	2.0	7
156	Aug. 22, 1991	9	42	7	38.26	-5.04	6	0.1	2	2	1.9	7
157	May 19, 1992	19	23	3	37.57	-6.02	10	0.1	3	1	2.4	7
158	July 4, 1994	13	38	47	37.63	-6.92	23	0.5	1	1	4.3	30
159	March 30, 1995	15	54	42	38.10	-6.53	11	0.6	1	1	3.8	17
160	April 11, 1995	6	42	20	38.43	-2.88	7	0.6	1	1	3.5	12
					Cantabrian Range							
161	Feb. 20, 1989	20	52	28	43.08	-5.11	5	0.5	1	2	3.7	7

Date, hour, minute, and second columns show the origin time parameters. Lat, long, and depth columns show the hypocentral coordinates. RMS, root-mean-square residual. *Erh* is the horizontal error. *Erz* is the vertical error. *M* is the magnitude. N Polarities is the number of polarities used for the focal mechanism determination.

*Events have been used only with *Giner's* [1996] technique.

principal stresses, respectively. The orientation is evaluated by Euler's angles that result in the transformation of the geographical system of reference into the one defined by the principal axes (σ_1, σ_2, σ_3). The mathematical quality of the solution is evaluated by the likelihood function normalized to the unity and the score. This last parameter is defined as the ratio between the number of polarities consistent with the tensor and the total number of polarities. Rivera and Cisternas's method is one of the most used procedures to estimate the stress tensor from a population of focal mechanisms [*Dorbath et al.*, 1991; *Delouis et al.*, 1993; *Lindo*, 1993; *De Vicente et al.*, 1996; *Fuenzalida et al.*, 1996; *Herraiz et al.*, 1996; *Goula et al.*, 1999]. In this study, more than 7000 trial sets, obtained with increments of 10° for Euler's angles and different solutions for the focal mechanisms, were used in each case to diminish the dependence of the solutions on the trial conditions.

The second method was a technique developed by *Giner* [1996] applying FPA methods to earthquake focal mechanisms. In our work, these fault population methods were the same as those used to analyze the recent fault data, in particular, the stress inversion method [*Reches*, 1987] and the slip model [*Capote et al.*, 1991]. This implies that mechanical restrictions to focal mechanisms should be imposed. It is worth noting that this method deduces which mechanical parameters better match the sample, instead of attributing values selected a priori. *Reches* [1987] proved that the methods that do not take into account the cohesion factor during the slip on the fault, according to Coulomb's law, assume that this parameter is null; that is, they impose a determined mechanical condition. At present, the consideration of the cohesion factor in the stress inversion is in progress, and the results will be improved when new physical data about rock friction are available.

Giner's [1996] technique begins with the application of a graphical-interactive program developed by *Cabañas et al.* [1996]. This program uses *P* polarities and azimuth and incidence angles to yield all the possible individual focal mechanisms that

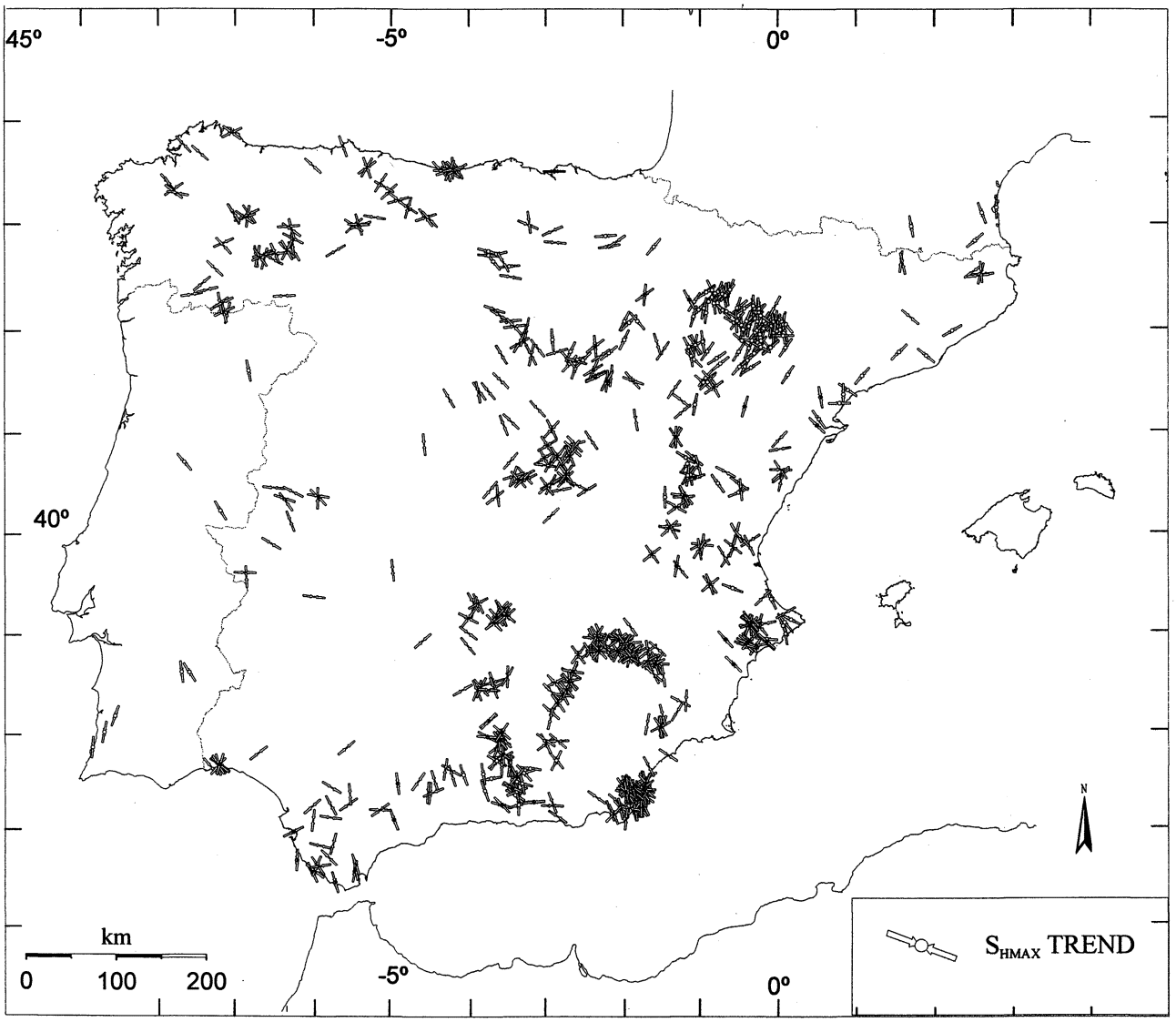

Figure 2. S_{Hmax} orientations obtained from geologic sites using the stress inversion method [*Reches et al.*, 1992].

satisfy a previously chosen score value. The discrimination of which one of the nodal planes corresponds to the fault has been done following the procedure developed by *De Vicente* [1988] and *Capote et al.* [1991] that uses the slip model [*Reches*, 1983]. In this way, a new population of possible fault planes for all the earthquakes is created. The resulting sample is analyzed with the fault population techniques in order to get one stress tensor and the directions of maximum horizontal compression that fit the sample. Then, these results are used to select only one focal mechanism for each seismic event, according to the angular error between the e_y directions and the K' values ($K' = e_y/e_z$). After that, the whole procedure is repeated to obtain one stress tensor and the e_y directions that fit the new focal mechanism population. Once the best stress tensor has been deduced and the mechanical characteristics and the individual incompatible mechanisms have been determined, all the focal mechanisms are plotted with the usual stereographical projection. The study ends with the application of the Lissage program [*Lee and Angelier*, 1994] to draw the trajectories of S_{Hmax}.

The whole methodology has been applied in two steps. Firstly, the Spanish peninsular territory has been divided into 12 zones. All of them, bar the Iberian Massif, are mainly based on the tectonic criteria of *Julivert et al.* [1972]. The Iberian Massif has been subdivided into four subzones (Northwest, Cantabrian Range, Central System, and Toledo and Sierra Morena Mountains) according to the tectonic units resulting from the alpine deformation (Figure 4). Geological and seismological data corresponding to each zone have been studied separately. Secondly, attention has been paid to a single set of data made out of the whole information corresponding to Spain and the results obtained for Portugal by *Ribeiro et al.* [1996]. This procedure allows us to obtain detailed knowledge in each zone as well as an overview of the stress distribution for the whole Iberian Peninsula. In addition, the comparison of the results for the upper

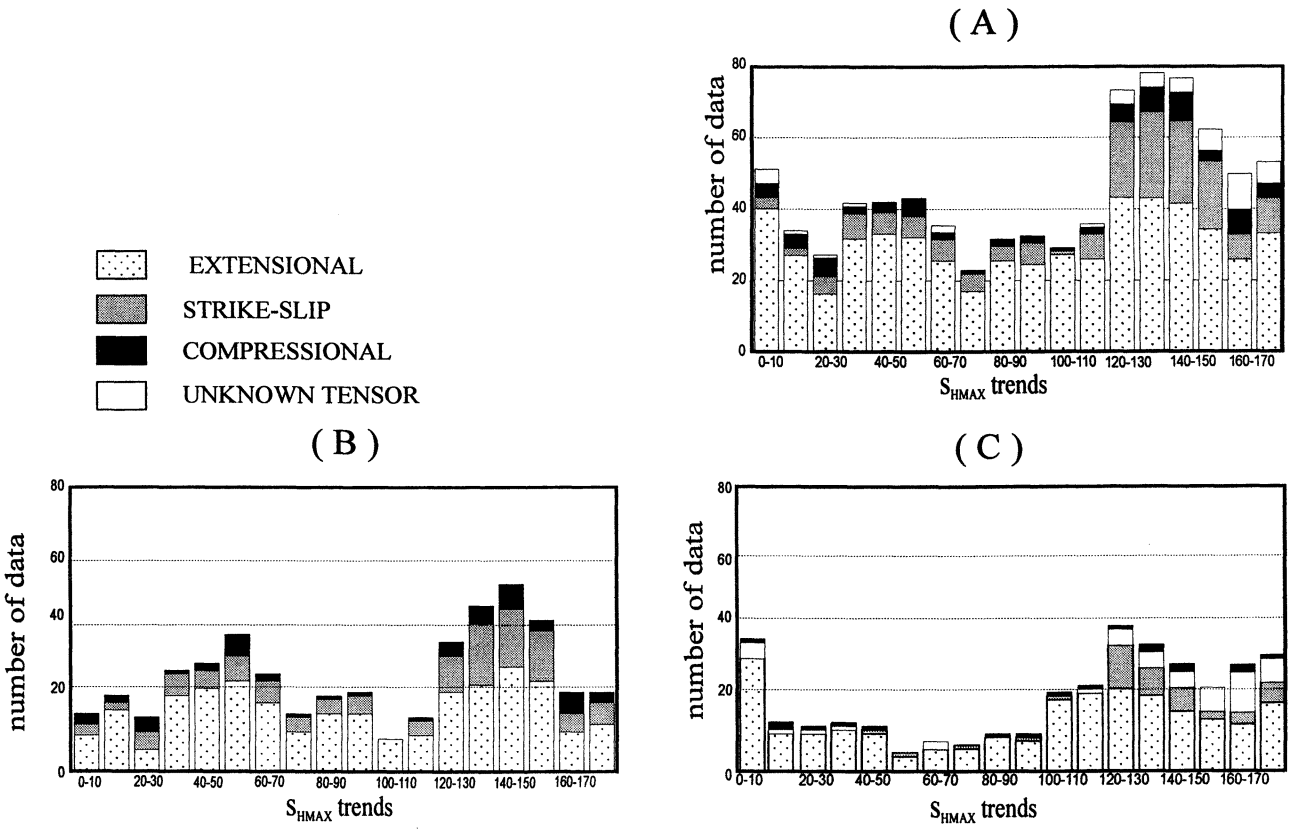

Figure 3. Type of stress tensor and histograms of the $S_{H\max}$ trends displayed in Figure 2. (a) All data. (b) Field data. (c) Bibliographic data.

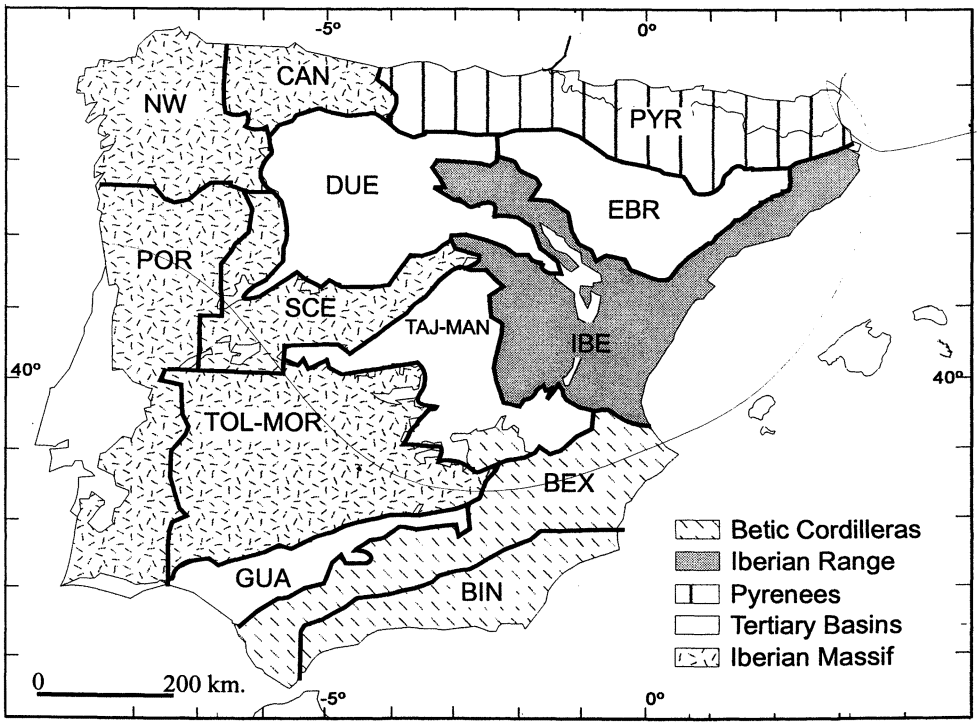

Figure 4. Distribution of areas with common tectonic characteristics selected to perform the analysis of regional stress tensors. BEX, External Units of the Betic Cordilleras; BIN, Internal Units of the Betic Cordilleras; CAN, Cantabrian Range; DUE, Duero Basin; EBR, Ebro Basin; GUA, Guadalquivir Basin; IBE, Iberian Range; NW, northwest Iberian Massif; POR, Portugal; PYR, Pyrenees; TAJ-MAN, Tajo Basin and La Mancha Plain; TOL-MOR, Toledo and Sierra Morena Mountains; SCE, Central System.

Table 4. Number of Geological Stations and Data Corresponding to the Areas With Similar Structural Characteristics

Zone	Field Data				Bibliographic Data	
	Number of Stations	Number of Data	Number of e_y Trends	Number of $S_{H\max}$ Trends	Number of Stations	Number of $S_{H\max}$ Trends
BEX	110	2487	143	135	55	69
BIN	42	893	58	51	86	95
NW	48	889	54	47	0	0
TAJ-MAN	44	1453	69	68	0	0
GUA	19	431	24	20	0	0
DUE	26	350	32	28	17	18
CAN	29	529	37	35	0	0
TOL-MOR	13	378	16	10	0	0
POR	0	0	0	0	10	10
IBE	41	873	56	46	118	119
PYR	16	243	17	13	8	8
EBR	2	18	2	2	30	31
SCE	19	226	23	19	0	0
Total	409	8770	531	474	324	350

Table 4 includes the number of orientations of the maximum shortening axis, e_y, and the maximum horizontal stress, $S_{H\max}$, obtained with the slip model [*De Vicente*, 1988] and the stress inversion method [*Reches et al.*, 1992], respectively. Zone abbreviations correspond to: BEX, External Units of the Betic Cordilleras; BIN, Internal Units of the Betic Cordilleras; CAN, Cantabrian Range; DUE, Duero Basin; EBR, Ebro Basin; GUA, Guadalquivir Basin; IBE, Iberian Range; NW, northwest Iberian Massif; POR, Portugal; PYR, Pyrenees; TAJ-MAN, Tajo Basin and La Mancha Plain; TOL-MOR, Toledo and Sierra Morena Mountains; SCE, central System. For locations, see Figure 4.

Miocene and Pliocene-Quaternary periods to the present-day stress field, allows us to sketch its temporal evolution. A detailed explanation of both data and methodology can be found in the work of *Herraiz et al.* [1998].

4. Regional and Dominant Stress Tensors in the Iberian Peninsula

The results of the World Stress Map [*Zoback*, 1992] have emphasized that the $S_{H\max}$ orientations can be uniform within the plates over distances up to 5000 km. These "regional" fields are usually accompanied by local modifications in the stress characteristics that can show a large variety of scales and magnitudes. Nevertheless, as *Rebaï et al.* [1992] pointed out, the changes of stress directions on a particular scale are consistent with the kinematics of the faults on the same scale. Western Europe, where both regional [*Müller et al.*, 1992] and local [*Rebaï et al.*, 1992] patterns of $S_{H\max}$ can be found, is a clear example of the existence of local variations in the frame of a broader uniform stress distribution. The results of our study seem to confirm this fact. In sections 4.1 and 4.2 we describe the recent and present-day stress tensors obtained both for the zones sketched in Figure 4 in which there were enough data to perform the analysis and for the whole Spanish mainland. These last tensors will be called "recent dominant tensor" and "present dominant tensor." Geological sites located within each zone and the number of $S_{H\max}$ trends obtained in each case are summarized in Table 4.

4.1. Recent Stress Tensors

In order to study the regional distribution of recent stress tensors, fault data of each zone have been analyzed using the stress inversion method [*Reches et al.*, 1992] and the bootstrap sampling technique. The obtained results are displayed in Figure 5. Tensors corresponding to Cantabrian Range and Ebro Basin zones are not included, because they were considered not well constrained. The solution for Duero Basin only represents its easternmost part (Almazán Basin), because the appropriate outcrops were found only in this area. The quality of the results logically depends on the number of data (Tables 1, 2, and 4), but when this is high, the $S_{H\max}$ can be considered accurately established. The results indicate a clear predominance of extensional stress tensors.

With the aim of deducing the dominant recent stress tensor for the whole Spanish mainland, the structural data were grouped in only one set and analyzed as a unique sample. The results are displayed in Figure 3a where a well-defined mode for $S_{H\max}$ trending 120°N-160°E can be noted. This mode can be also observed when field and bibliographic data are plotted in a separated way (Figures 3b and 3c, respectively). A clear predominance of extensional tensors ($\sigma_1 = \sigma_z$) and a much lower number of compressional stress tensors are noticeable in Figures 3a-3c. Trajectories obtained using *Lee and Angelier's* [1994] technique to interpolate the data that follow the predominant NW-SE orientation are displayed in Figure 6.

4.2. Present-Day Stress Tensors

Rivera and Cisternas's [1990] method and *Giner's* [1996] technique have been tried in each zone although the low seismicity of some of the zones has limited their simultaneous application to seven areas: Northwest, Pyrenees, Iberian Range, Tajo Basin and La Mancha Plain, Toledo and Sierra Morena Mountains, External Betics, and Internal Betics. The results are listed in Table 5 and appear in Figures 7-9. Figures 7 and 8 describe the tensors and the focal mechanisms, respectively, given by Rivera and Cisternas's method, whereas Figure 9 shows the tensors obtained with Giner's procedure. In some cases, more than one stress tensor per region was estimated with this last technique.

Directions for the maximum horizontal stress $S_{H\max}$ obtained with both techniques are systematically coincident. Concerning

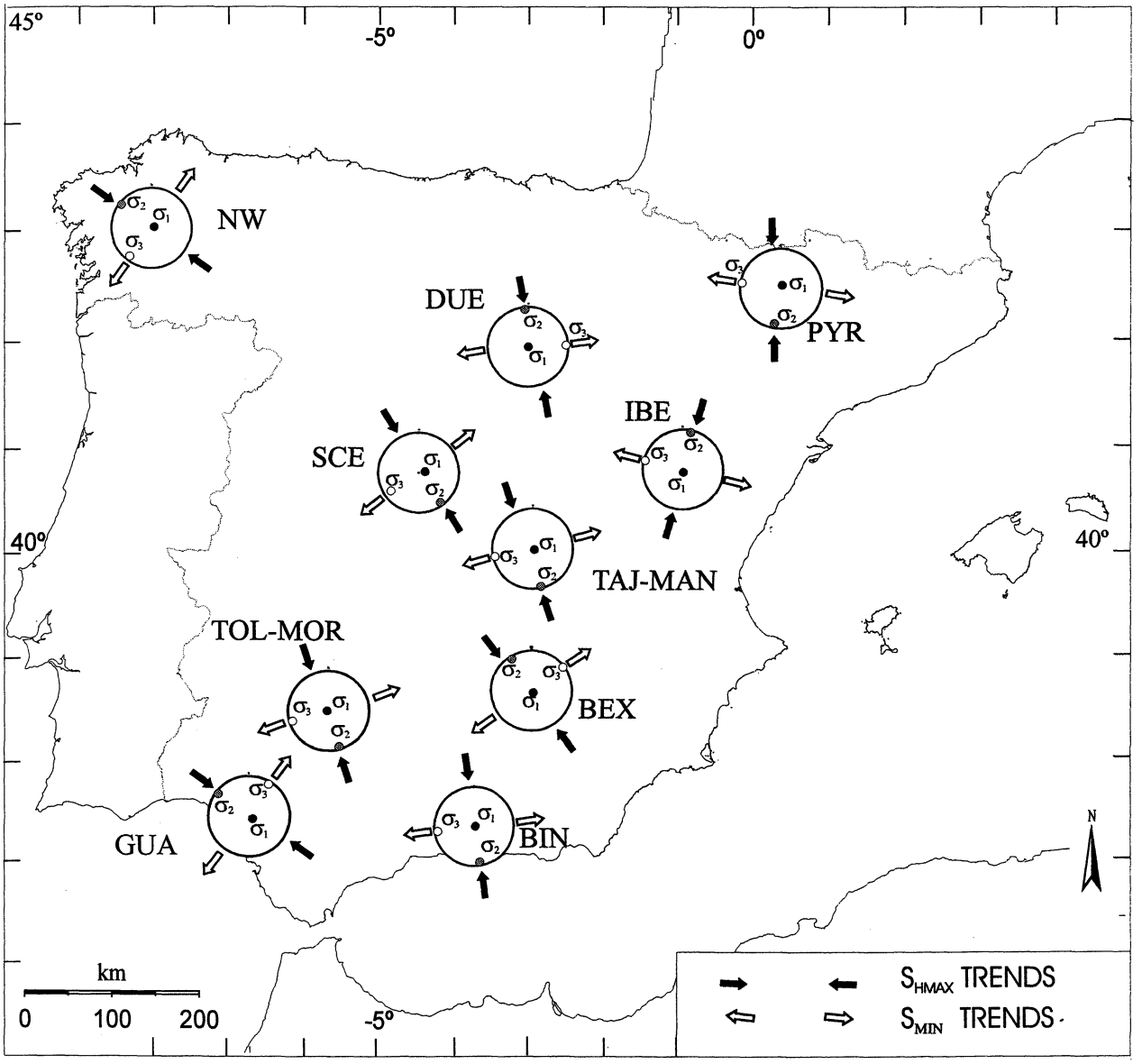

Figure 5. Recent regional stress tensors corresponding to some of the zones indicated in Figure 4. The tensors have been obtained using the stress inversion method [*Reches et al.*, 1992].

the stress tensors, both the slip model and the inversion stress method, which are the basis of *Giner's* [1996] technique, assume mechanical requirements. These conditions constrained the possible solutions in a different way from that of *Rivera and Cisternas's* [1990] method, whose aim is to find mean tensors. These two points of view are complementary to each other and look for different objectives. The aim of Rivera and Cisternas's method is to determine the stress tensor capable of explaining every focal mechanism of the earthquakes that have taken place in a zone assumed tectonically homogeneous. This method does not try to find focal mechanisms with the greatest score but looks for the tensor parameters and the focal mechanisms that maximize the probability that the polarities are placed correctly according to the radiation pattern of each fault plane solution. Therefore the objective is to optimize the likelihood function, not the score. On the contrary, the fault population methods on which Giner's technique is based, are oriented to find one or several tensors mechanically different. With this approach the possible individual focal solutions are stressed. If there exists a fault that is not mechanically compatible with the average solution, the method keeps high scores but indicates the existence of a heterogeneity between the deformation conditions of this mechanism and those corresponding to the others. As a consequence, Rivera and Cisternas's method is prone to choose only one solution of those deduced by Giner's procedure or, as it happens in our study for the Pyrenees and the External Betics, finds an intermediate solution. It has already been observed that when deformation is heterogeneous, two or three tensors may be

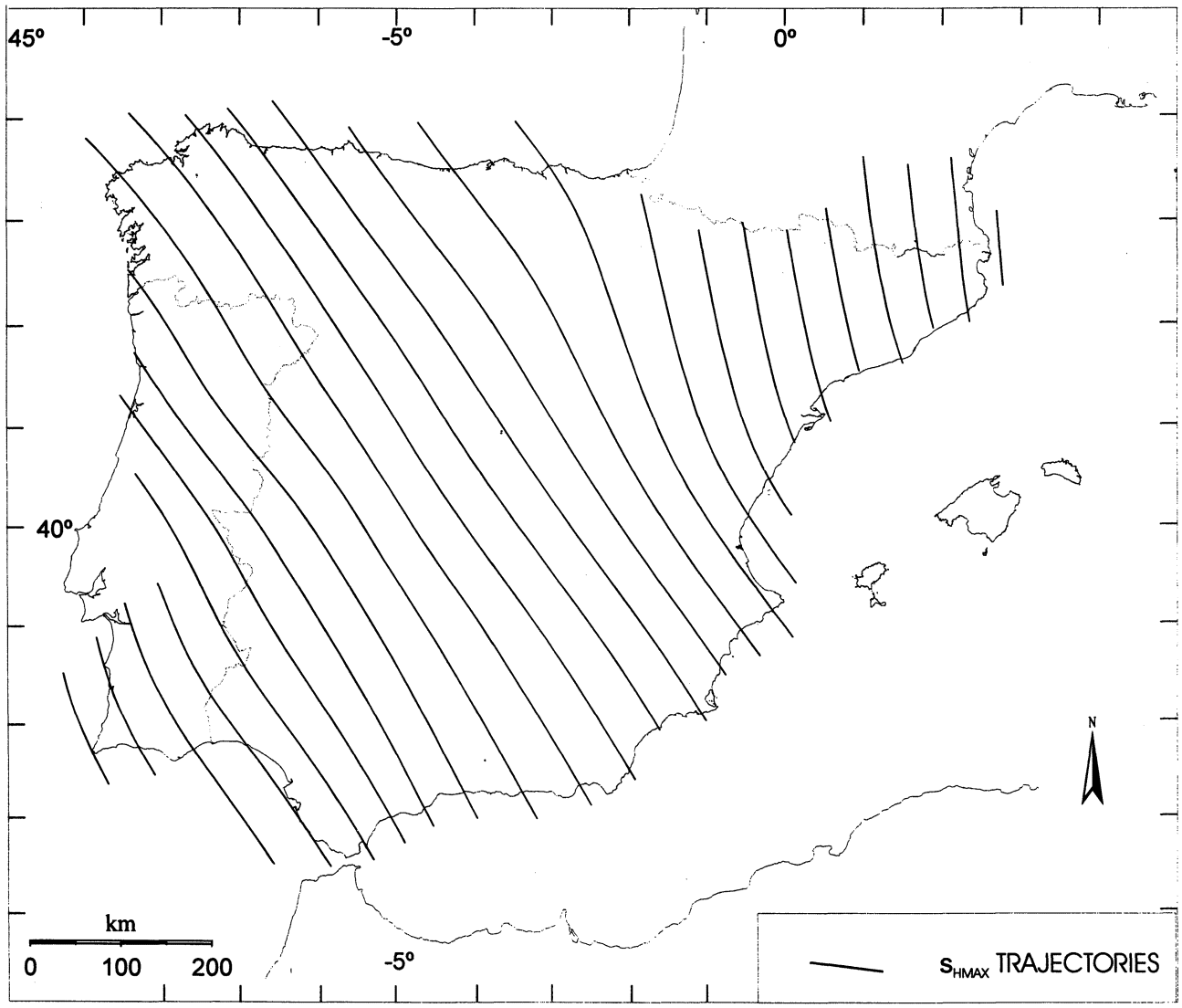

Figure 6. $S_{H\max}$ trajectories drawn applying the *Lee and Angelier* [1994] interpolation program to data that follow the NW-SE predominant orientation which appears in Figure 3.

separated for microseismic activity of aftershock sequences. These tensors are coaxial in the range of uncertainties, and one of them is in agreement with the regional state of stress [*Mercier and Carey-Gailhardis*, 1989; *Carey-Gailhardis and Mercier*, 1992].

With these approaches the results given by *Rivera and Cisternas'*s [1990] method for the different zones (Figure 7) are strike-slip stress tensors except for the Internal Betics and the Iberian Range, where triaxial extensions are present. *Giner'*s [1996] technique (Figure 9) indicates compression close to the uniaxial type in Sierra Morena and External Betics; extension in the Iberian Range and the eastern Pyrenees, and a strike-slip regime in the Northwestern sector and the Tajo Basin-La Mancha Plain. All the zones except the Pyrenees and the Internal Betics show a NW-SE compression that dominates in both recent and present stress states. The western Pyrenees and the External and Internal Betics show two stress tensors that are mechanically incompatible.

The joint application of *Rivera and Cisternas'*s [1990] method to the sample of 156 events indicates a maximum compressional axis oriented NW-SE and a strike-slip regime with a shape factor R equal to 0.51 (Figure 10). The score is 0.77, and the likelihood is 0.85. This low value reflects the heterogeneity of the sample.

Application of *Giner*'s [1996] technique to the same sample extended to 161 events reveals the presence of an absolute maximum of $S_{H\max}$ oriented N135°E and a relative maximum trending N30°E (Figure 11). As it can be observed in the histogram of fault types and $S_{H\max}$ orientations (Figure 12), both maxima show a large variety of associated faults, those of reverse type being the most numerous. This fact represents a disagreement with the geological results obtained from field sites

Table 5. Shape Factors, R= $(\sigma_2-\sigma_3)/(\sigma_1-\sigma_3)$, and Maximum Horizontal Stress Directions, S_{Hmax}, Obtained in the Areas Plotted in Figure 4 in Which There Were Enough Data to Analyze the Regional Stress Tensor

	Giner [1996] Method				Rivera-Cisternas [1990] Method			
Zone	R	S_{Hmax}	Score	Quality	R	S_{Hmax}	Score	Quality
PYR	0.04 (SS) 0.63 (E) 0.24 (E)	14 (1) 15 (2) 111 (2)	0.96 0.94 0.98	A	0.47 (SS)	5 (1)	0.86	A
NW	0.67 (SS)	140 (1)	0.82	A	0.86 (SS)	155 (1)	0.77	A
TAJ-MAN	0.21 (SS)	143 (1)	0.85	B	0.36 (SS)	130 (1)	0.75	A
TOL-MOR	0.27 (C)	115 (1)	0.89	A	0.70 (C)	157 (1)	0.83	A
IBE	0.58 (E)	163 (2)	0.86	A	0.60 (E)	160 (2)	0.86	A
BEX	0.05 (SS)	136 (1)	0.90	A	0.37 (SS)	130 (1)	0.80	A
BIN	0.10 (E) 0.17 (C) 0.06 (E)	121 (2) 11 (1) 166 (2)	0.91 0.83 0.87	A	0.49 (E)	160 (2)	0.78	A

Letters associated with R values indicate the tensor characteristics: E, extensional; SS, strike slip; and C, compressional. Numbers in parenthesis indicate the axis defining the corresponding direction. Quality ranking follows *Zoback*'s [1992] criterium.

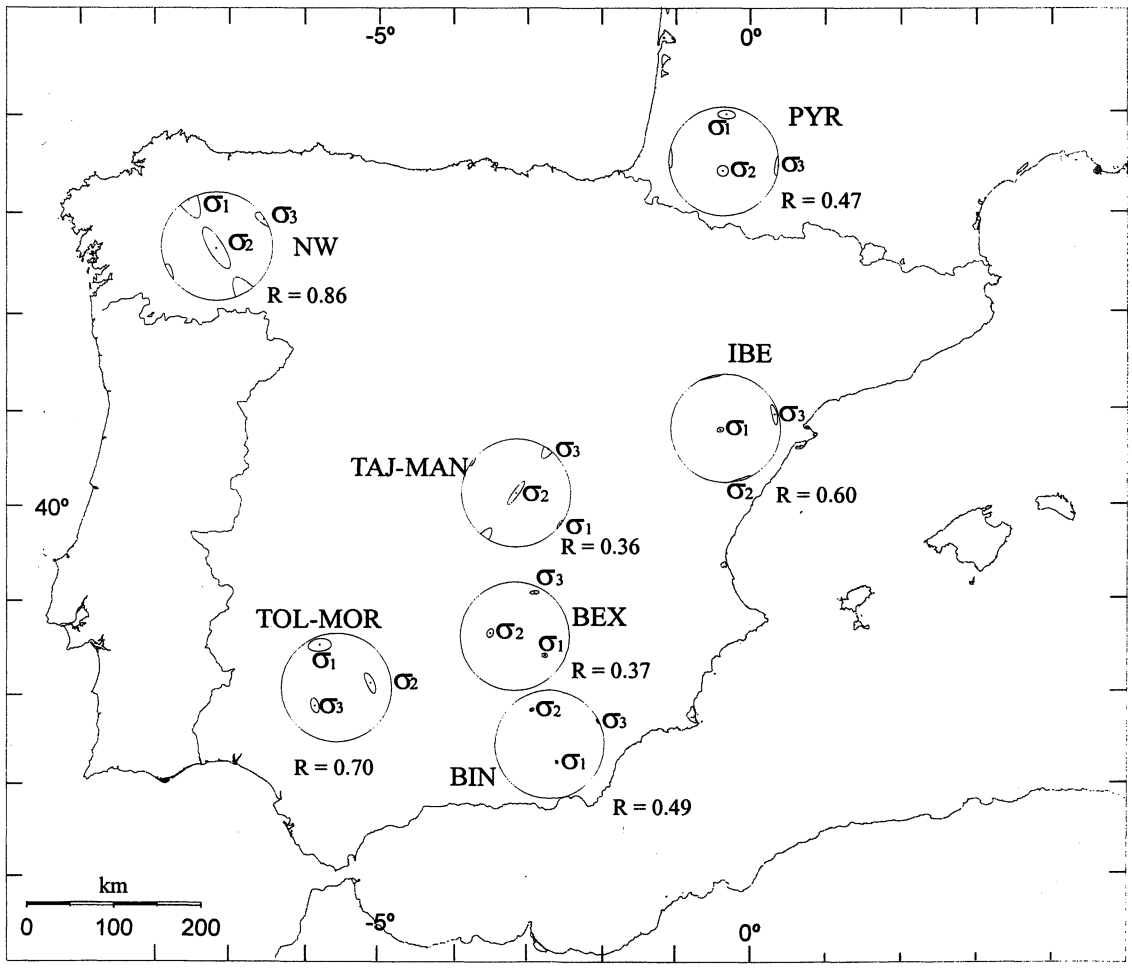

Figure 7. Present-day regional stress tensors obtained with the technique developed by *Rivera and Cisternas* [1990]. The shape factor (R=$(\sigma_2-\sigma_3)/(\sigma_1-\sigma_3)$) for each region is also shown.

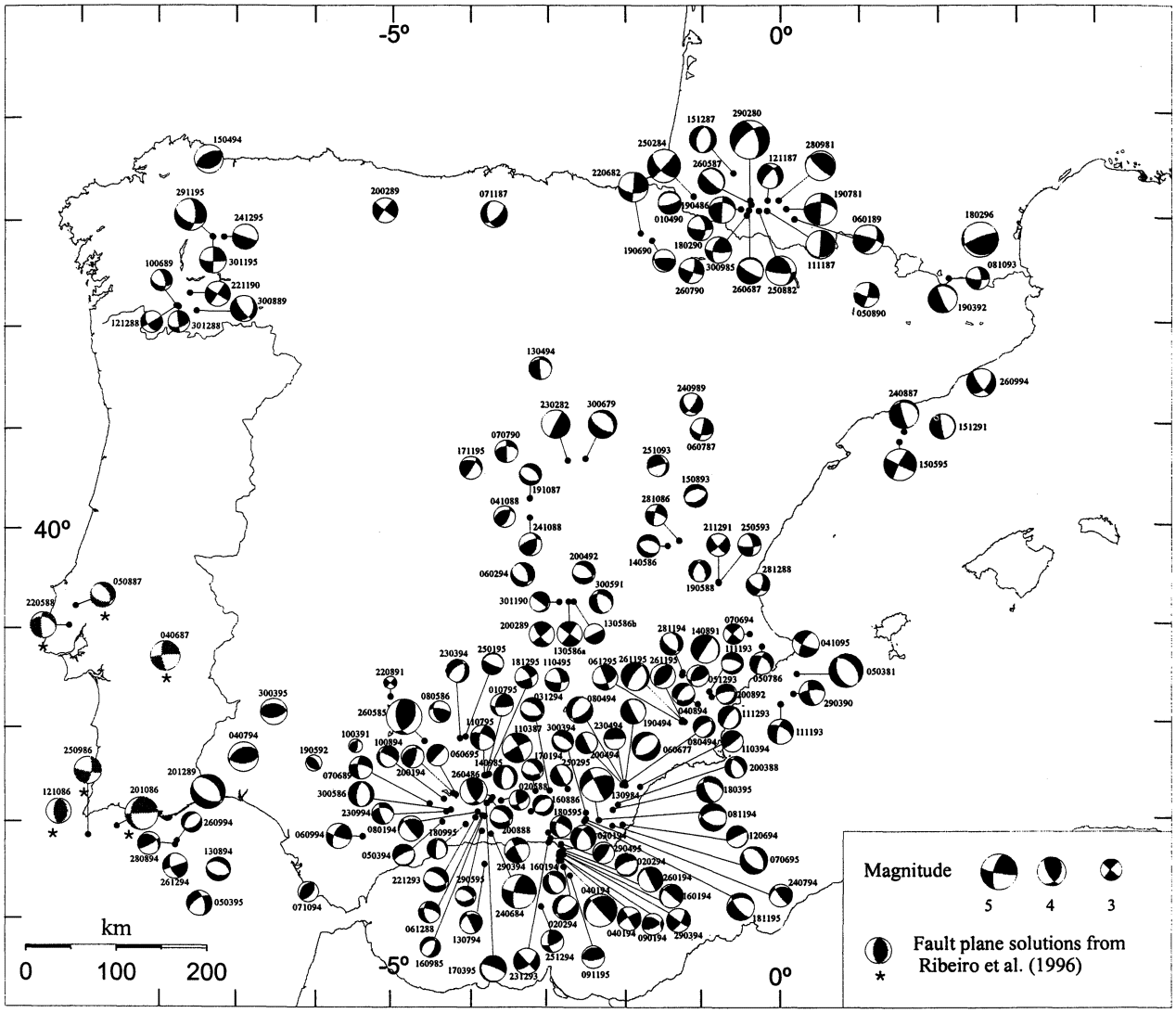

Figure 8. Focal mechanisms of the 156 individual events computed using the method of *Rivera and Cisternas* [1990] (see the corresponding tensors in Figure 7). The six mechanisms taken from *Ribeiro et al.* [1996] are also plotted and distinguished with a star. The fault plane solutions are shown in a lower hemisphere Schmidt projection, and numbers close to each representation indicate the event date.

that showed a clear predominance of normal faults. A possible explanation will be discussed in section. 5.

Focal mechanisms obtained with *Giner's* [1996] method together with the $S_{H\max}$ trajectories of the dominant NW-SE stress field are displayed in Figure 13. Figure 13 also includes the six mechanisms obtained by *Ribeiro et al.* [1996], which have been used to draw stress trajectories in Portugal. The stress method [*Reches et al.*, 1992] applied to the whole population of mechanisms yields two tensor types with a common orientation for $S_{H\max}$ (Figure 14). The first one (Figure 14a) corresponds to an extensional regime ($\sigma_1 = \sigma_z$) and explains 80 mechanisms. The shape factor R is 0.07, pointing to a triaxial, close to radial extension. The second tensor (Figure 14b) explains 58 mechanisms and corresponds to a strike-slip regime (σ_2 vertical); the stress ratio $R = 0.14$ indicates high reverse components. The scores of these solutions are 0.87 and 0.88, respectively.

5. Discussion and Conclusions

The application of fault population analysis together with focal mechanism determination makes it possible to obtain a broader and complete picture of the recent and present-day stress fields but requires a large number of data and a good spatial distribution. In our case this problem has been important because of the low seismicity of several zones in the Iberian Peninsula and the uneven geographical distribution of the outcrops of recent rocks. Nevertheless, the amount of geological and seismological data used in the study allows us to consider our results well founded, especially when they have been obtained with different techniques. It is necessary to consider that data taken in the measurement sites only represent the fracture characteristic near the surface, whereas the information obtained from earthquake analysis casts some light on the stresses acting

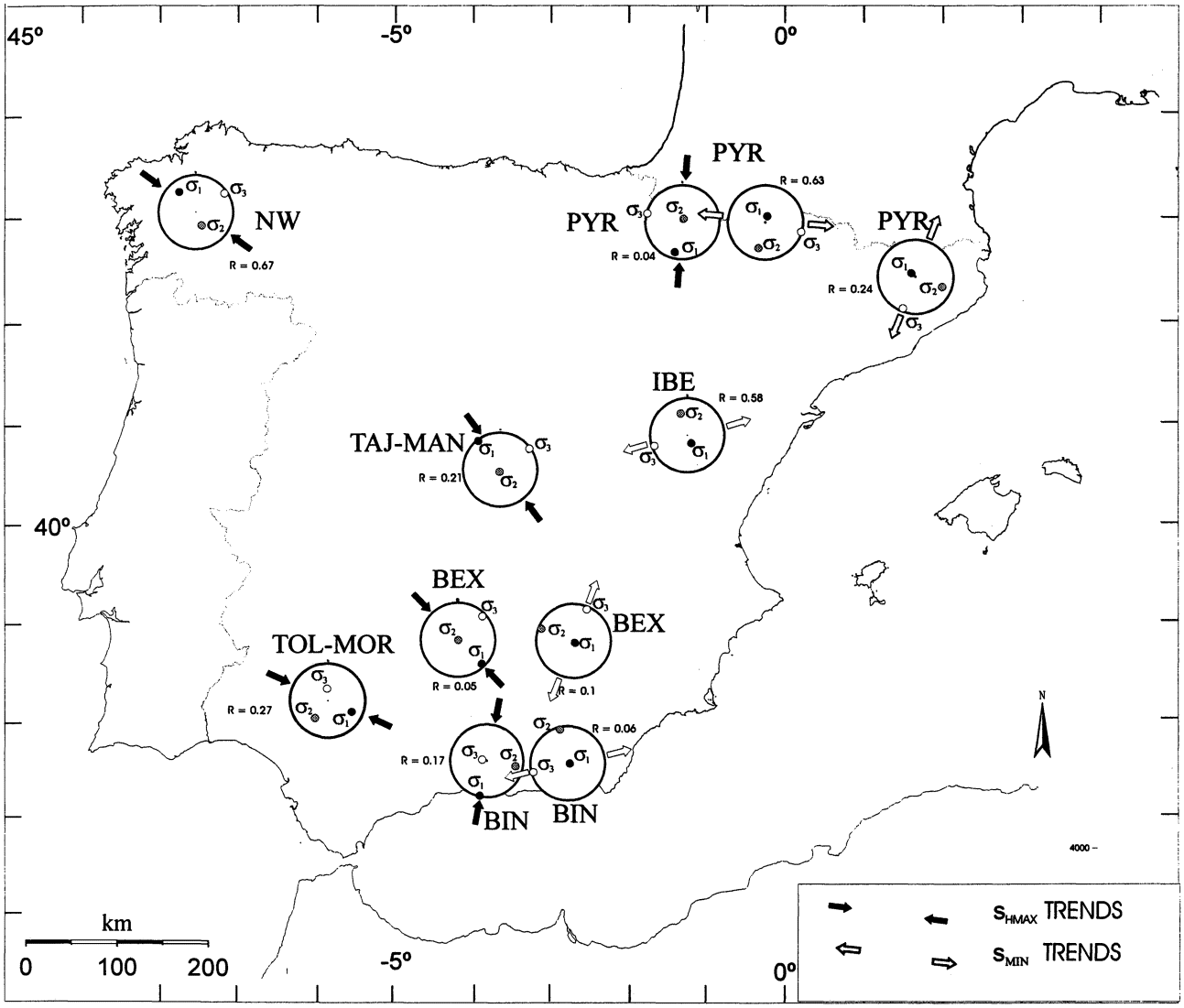

Figure 9. Present-day regional stress tensors deduced by means of *Giner's* [1996] method for some areas of Figure 4.

on the crust, down to 30 km deep. This fact can explain the different stress regime obtained from geological and seismic data, but this argument must be verified in the future by improving the hypocentral locations and increasing the number of seismic data. Microseismicity studies carried out in specific areas can be a useful tool to achieve this purpose [see, e.g., *Herraiz et al.*, 1996]. A change of the stress tensor in time can not be totally ruled out either, although the results obtained in different zones indicate the continuity of the stress distribution from late Miocene to present time.

The comparison of the results obtained for the whole Iberian Peninsula to those corresponding to individual zones makes clear the existence of (1) a primary pattern for the stress field characterized by the constancy of the $S_{H\max}$ NW-SE direction and (2) the possibility of some regional stress fields associated to specific tectonic or geologic features. These fields can be assimilated to "first-," and "second-," order patterns respectively, according to the terminology proposed by *Zoback* [1992]. The primary pattern seems to reflect the stresses generated by the convergence between African and Eurasian plates and the W-E ridge push originated in the middle Atlantic rift. N-S to NE-SW orientations of $S_{H\max}$ in NE Spain (see Figure 2) are not consistent with the western European mean direction, suggesting the occurrence of tectonic forces coming from the Pyrenean zone [*Cortés and Maestro*, 1998]. Secondary stress fields in the Pyrenees and Betics (Figure 9) can be related to topographic highs and upper crust structures.

The results obtained for the Pyrenees are complex. For the whole chain, *Rivera and Cisternas's* [1990] method defines a wrench regime with the shape factor R=0.47 and $S_{H\max}$ in N-S direction. For the western part, *Giner's* [1996] technique gives two coaxial stress tensors. The predominant one points out a strike-slip regime with a horizontal compression (σ_1) at N14°E and R = 0.04. This solution is analogous to that given by Rivera and Cisternas's method. The second tensor is extensional and presents $S_{H\max}$ oriented N15°E. The shape factor is 0.63. In the

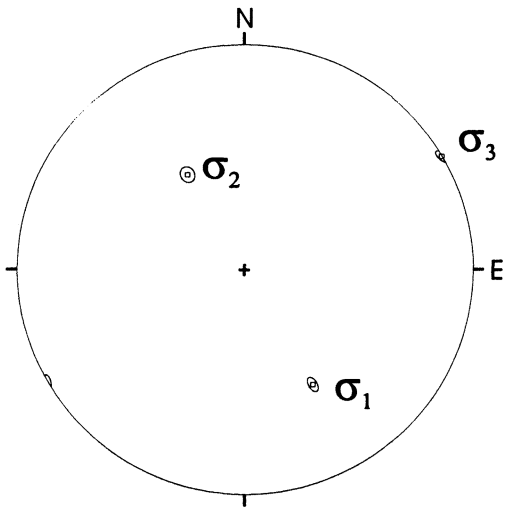

Shape Factor :	R=0.51
Orientation :	σ_1 :azimuth = 150° dip= 41°
	σ_2 :azimuth = 330° dip= 49°
	σ_3 :azimuth = 60° dip= 0°
Quality:	Likelihood=0.85
	Score=0.77

Figure 10. Mean stress tensor representation obtained by the joint inversion of the whole main set of earthquakes (156 events listed in Table 3) using the technique developed by *Rivera and Cisternas* [1990].

eastern Pyrenees the same procedure indicates an extensional regime with a $S_{H\max}$ in the N111°E direction, but in this case the low number of events analyzed (only four) diminishes the reliability of the result. Recently, *Goula et al.* [1999] have found a strike-slip or compressional stress tensor with $S_{H\max}$ in the N-S

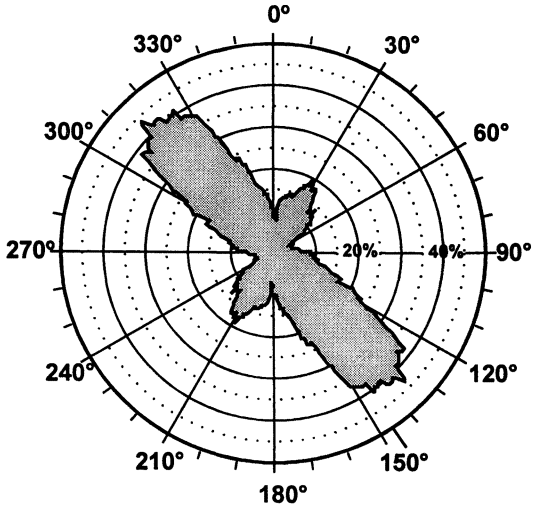

Figure 11. $S_{H\max}$ rose diagram from the enlarged population of seisms with calculated focal mechanism (161 events). The modal value of $S_{H\max}$ orientation is N135°E.

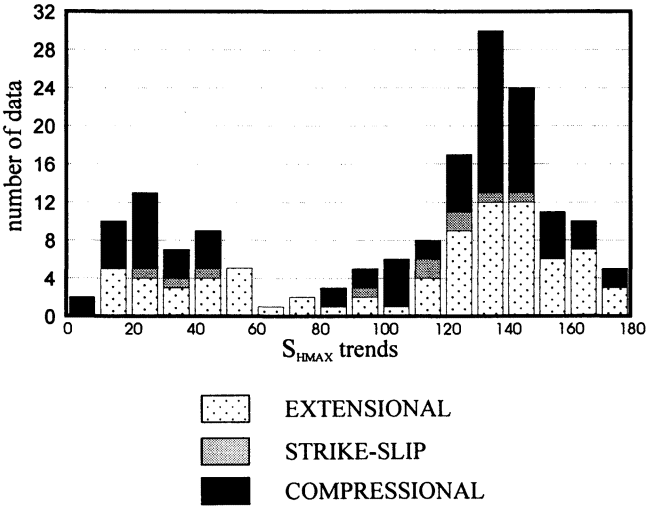

Figure 12. Stress tensor types and histogram of $S_{H\max}$ orientations deduced from the total population of seisms (161 events) with calculated focal mechanism.

direction for a zone that includes the NE of Spain and the south of France. This solution was obtained considering 21 geological sites and 18 earthquakes. Although this variety of results shows that the stress state in the Pyrenees is not well understood yet, the existence of an acting N-S compression can be considered well established.

A situation similar to that in the western Pyrenees can be found in the External Betics, where 33 events have been analyzed. *Giner's* [1996] technique gives two different solutions: one compressive (R=0.05) and another extensive (R=0.10). Both have a very similar orientation for $S_{H\max}$. *Rivera and Cisternas's* [1990] method indicates a strike-slip stress tensor and a majority of normal focal mechanisms even though several clearly defined reverse solutions have been already found (Figure 8).

In the Internal Betics the application of *Giner's* [1996] method to a sample of 47 earthquakes also provides two solutions that are not mechanically compatible. The predominant solution shows a compressive stress tensor with R = 0.17. The σ_1 component is located N11°E. The nodal planes are interpreted as reverse faults, and they do not show a defined trend. The second solution corresponds to an extensional stress tensor close to radial (R=0.06), although in this case the interpretation of the nodal planes suggests the existence of normal faults with NW-SE orientation. As has been already commented on in section 4.2, in this zone *Rivera and Cisternas's* [1990] method gives only one solution which is analogous to the extensional stress tensor deduced by means of Giner's procedure. The simultaneous presence of normal and reverse faults can be explained as a topographic effect: the creation of an important relief generated by compression may induce extensional stresses.

For the other zones where the joint application of both methodologies has been possible (Northwest, Iberian Range, and Toledo and Sierra Morena Mountains), *Giner's* [1996] technique obtains only one tensor (Figure 9). In each case the orientation of $S_{H\max}$ agrees well with that given by *Rivera and Cisternas's* [1990] method.

The temporal evolution of stress fields in the Iberian Peninsula has been locally studied considering the sites where it

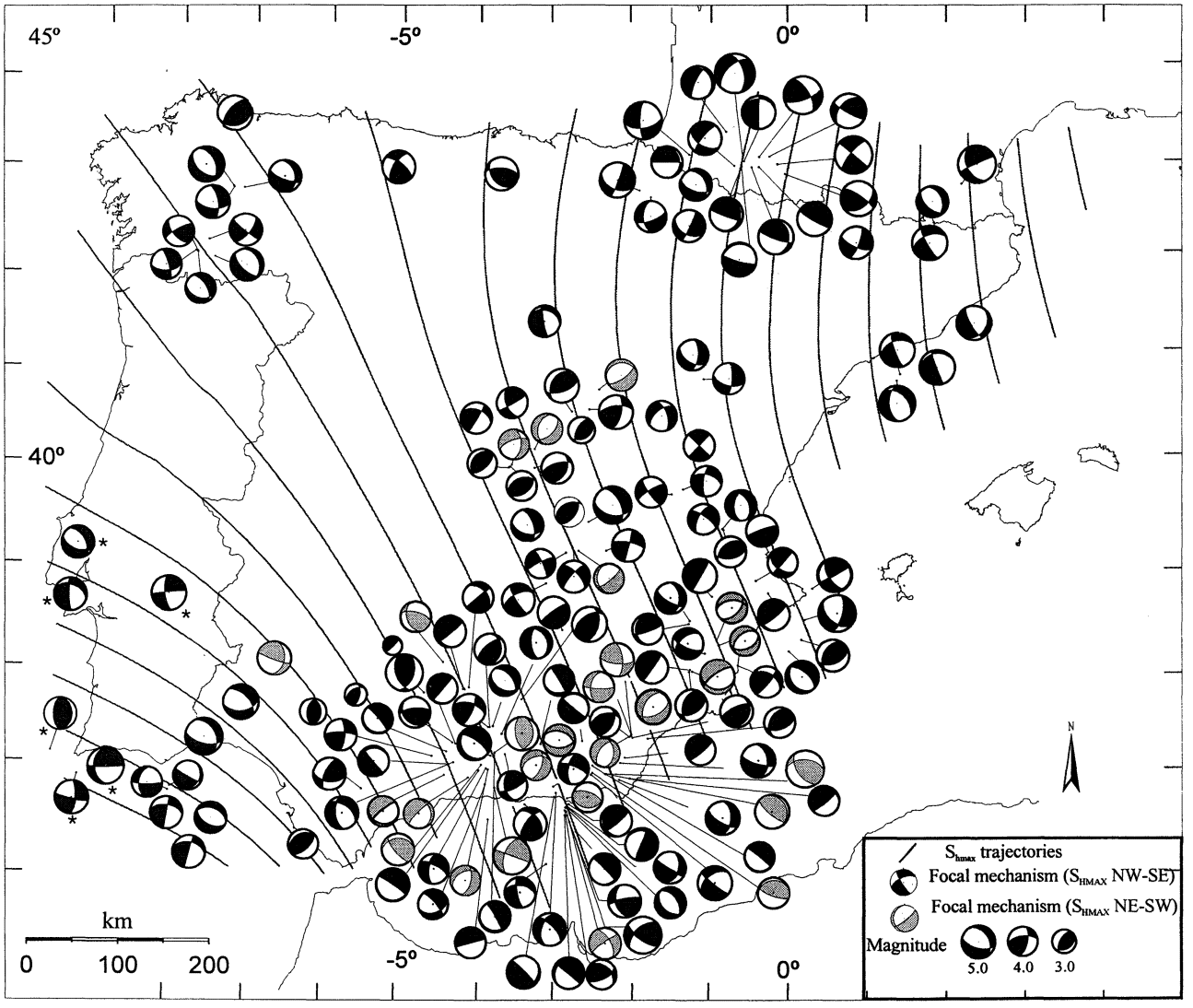

Figure 13. Focal mechanisms obtained using *Giner*'s [1996] method or taken from *Ribeiro et al.* [1996] (starred mechanisms). Fault plane solutions are shown in a lower hemisphere Schmidt projection. $S_{H\max}$ trajectories have been drawn interpolating local stress information deduced from focal mechanism fault planes and using the *Lee and Angelier*'s [1994] program. Shaded mechanisms represent solutions with $S_{H\max}$ located NE-SW. Solid focal mechanisms indicate solutions with $S_{H\max}$ oriented NW-SE.

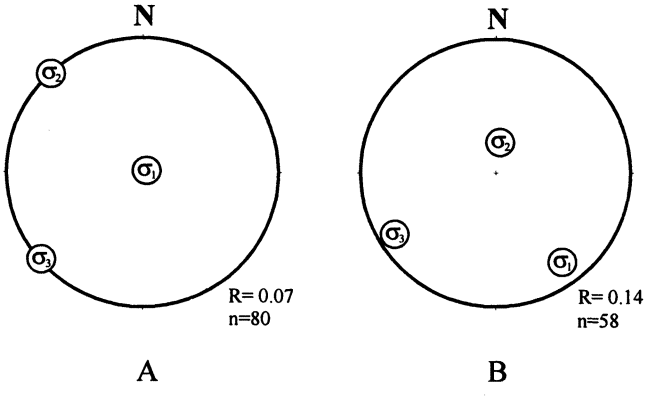

was possible to find fractures that affect both upper Miocene and Pliocene-Quaternary materials. In these cases the fault sample has been divided into two groups according with the deformation age. The results obtained after applying the stress inversion method to these populations show stress tensors that are similar for both ages (see the two examples in Figure 15). Nevertheless, the NNW-SSE compression in the Tajo Basin–La Mancha Plain

Figure 14. Stereographic plot of mean stress tensors obtained applying the stress inversion method [*Reches et al.*, 1992] to the population of 161 focal mechanisms. (a) Extensional regime explaining 80 focal mechanisms. (b) Strike-slip solution that explains 58 focal mechanisms.

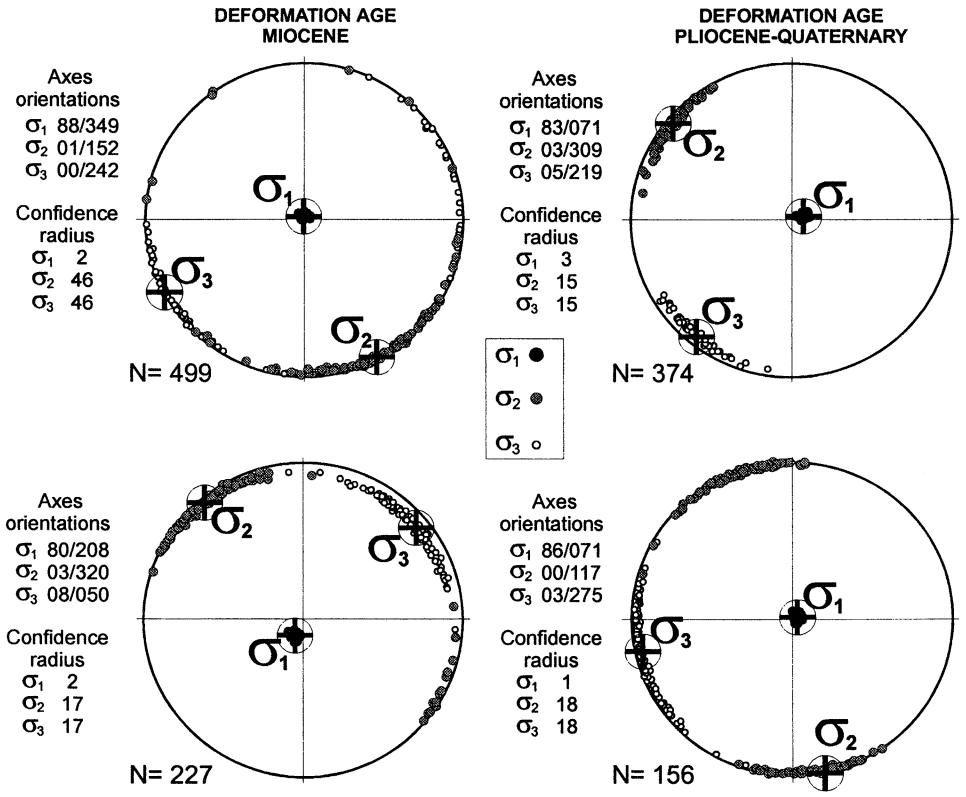

Figure 15. Results obtained applying the stress inversion method [*Reches et al.*, 1992] to faults of the (top) Northwest area and (bottom) Toledo-Sierra Morena area. Results are grouped according to the deformation age. The orientation of the main axes ($\sigma_1, \sigma_2, \sigma_3$) and the corresponding confidence radius are indicated. N represents the number of data. Temporal continuity of the stress orientation can be easily noticed.

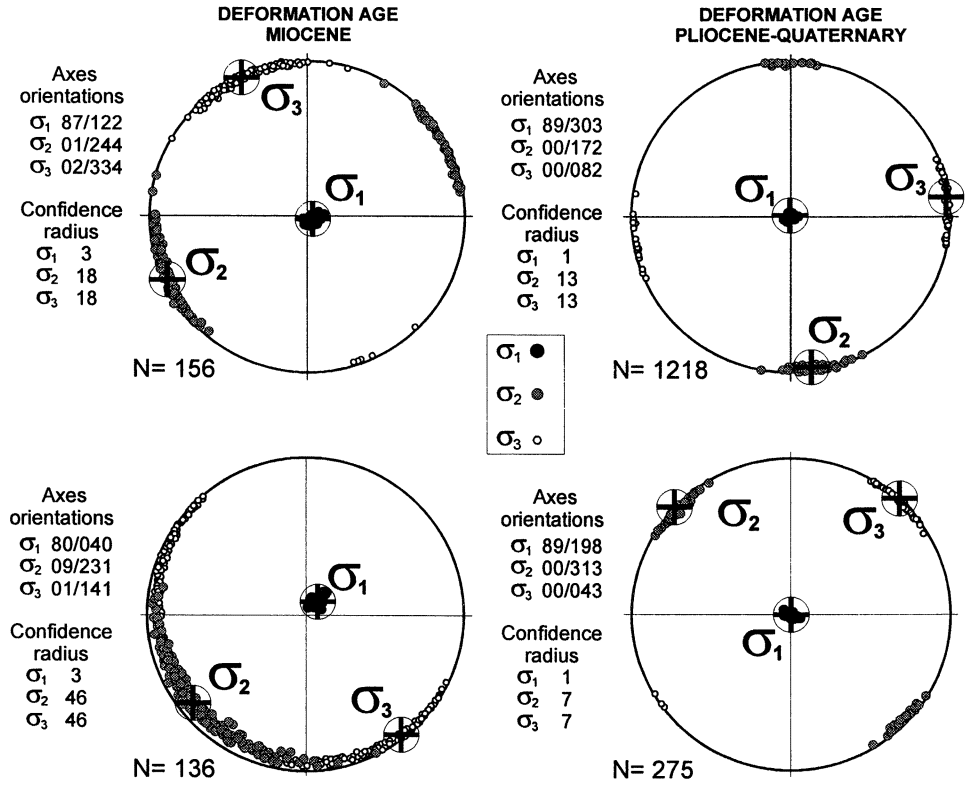

Figure 16. Results obtained applying the stress inversion method [*Reches et al.*, 1992] to faults of the (top) Tajo Basin-La Mancha Plain area and (bottom) Guadalquivir Basin area. Results are grouped according to the deformation age. The orientation of the main axes (σ_1, σ_2, σ_3) and the corresponding confidence radius are indicated. N represents the number of data. The results for the Pliocene-Quaternary data show a better definition of the NNW-SSE compression.

and Guadalquivir Basin zones is more defined for the Pliocene-Quaternary period (Figure 16). The last one involves switching of the σ_2 and σ_3 axes, a phenomenon recognized as well in the Cantabrian and Pirenean zones. On the other hand, compressional tensors registered in Pliocene-Quaternary deposits are very scarce. At the same time, in sites where compressional and extensional tensors are found together, extensional tensors are usually younger. This suggests a general trend from compressional to extensional regime for the whole Iberian Peninsula (except for the Betic Chain) during the Miocene-Quaternary times. Finally, a broader picture referred to the whole Spanish mainland can be reached comparing the present-day $S_{H\max}$ trajectories displayed in Figure 13 with those corresponding to the main $S_{H\max}$ trend for the dominant recent stress tensor (Figure 6). In both cases the trajectories have been drawn following *Lee and Angelier's* [1994] technique and using large interpolation radii due to the unequal data distribution. As these large values tend to smooth the curves, changes in $S_{H\max}$ orientations can be steeper. In any case, the comparison of both maps indicates that the main trends of the stress field in the Iberian Peninsula have remained almost invariable at least since the upper Miocene.

Summarizing the results, we can conclude that the Iberian Peninsula is undergoing a NW-SE compression except for the northeastern part (Pyrenees, Ebro Basin, and Iberian Chain), where it is mainly N-S to NE-SW, and the Gulf of Cádiz, where the direction seems to be E-W. *Rivera and Cisternas's* [1990] method allows us to obtain a dominant stress regime of strike-slip type. Results of *Giner's* [1996] procedure indicate the same regime for the intraplate zones of the Iberian Peninsula, whereas it shows the presence of two stress tensors in the areas closest to the Iberian plate borders: one of compressional character and other of extensional. The recent (since upper Miocene) stress tensor points to a dominant compression oriented 120°N-140°E, similar to the present-day field, together with another stress tensor of 30°N-60°E direction. The predominant type of faults is normal. When the number of geological sites is sufficient, the orientation of the maximum horizontal compression is well defined and agrees with that deduced from seismicity data.

Acknowledgments. We are very grateful to the following institutions, which have facilitated data and information: Instituto Geográfico Nacional, Instituto Andaluz de Geofísica y Prevención de Desastres Sísmicos, Real Instituto y Observatorio de la Armada, Institut Cartográfic de Catalunya, Instituto de Meteorología (Lisbon, Portugal), and Institut de Physique du Globe (Strasbourg, France). We also want to express our gratitude to Armando Cisternas and Luis Rivera for their continuous advice during the Sigma project. E. Buforn and F. Vidal kindly provided us with information on focal mechanisms. The help from Ramón Vegas, Diego Córdoba, Alfonso Muñoz-Martín, Noemí Casero, and Raúl Pérez has been very efficient at different steps of the work. This research has been supported by the Consejo de Seguridad Nuclear and the Empresa Nacional de Residuos Radioactivos S.A.

References

Angelier, J., and P. Mechler, Sur une méthode graphique de recherche des contraintes principales également utilisable en tectonique et sismologie: La méthode des dièdres droits, *Bull. Soc. Geol. Fr.*, *19*(6), 1309-1318, 1977.

Arlegui, L. E., Diaclasas, fallas y campo de esfuerzos en el sector central de la Cuenca del Ebro: Relación con el campo de esfuerzos neógenos, tesis doctoral, Univ. de Zaragoza, Zaragoza, Spain, 1996.

Benkhelil, J., Etude tectonique de la terminaison occidentale des Cordilleres Betiques [Espagne], thèse de doctorat, Univ. de Nice, Nice, France, 1976.

Bott, M. H. P., The mechanism of oblique-slip faulting, *Geol. Mag.*, *96*, 109-117, 1959.

Buforn, E., C. Sanz de Galdeano, and A. Udías, Seismotectonics of the Ibero-Maghrebian region, *Tectonophysics*, *248*, 247-261, 1995.

Cabañas, L., R. Lindo, and M. Herraiz, MF96: Un programa interactivo para la determinación gráfica de mecanismos focales, *Geogaceta*, *20*(6), 1377-1379, 1996.

Capote, R., G. De Vicente, and J. M. González-Casado, An application of the slip model of brittle deformations to focal mechanism analysis in three different plate tectonics situations, *Tectonophysics*, *191*, 399-409, 1991.

Carey, E., Recherche des directions principales de contraintes associées au jeu d'une population de failles, *Rev. Geol. Dyn. Geogr. Phys.*, *21*, 57-66, 1979.

Carey, E., and M. B. Brunier, Analyse théorique et numérique d'un modèle mécanique élémentaire appliqué à l'étude d'une population de failles, *C.R. Acad. Sci. Ser. D*, *279*, 891-894, 1974.

Carey-Gailhardis, E., and J. L Mercier, Regional state of stress, fault kinematics and adjustments of blocks in a fractural body of rock: Application to the microseismicity of the Rhine graben, *J. Struct. Geol.*, *14*(8/9), 1007-1017, 1992.

Casas, A. M., El frente norte de las Sierras de Cameros: Estructuras cabalgantes y campo de esfuerzos, tesis doctoral, Univ. de Zaragoza, Zaragoza, Spain, 1990.

Colomer, M., Estudi geológic de la vora sud-oest de la fosa de Calataiud-Daroca, entre Villafeliche i Calamocha, tesis de licenciatura, Univ. de Barcelona, Barcelona, Spain, 1987.

Cortés, A. L., and A. Maestro, Análisis de los estados de esfuerzos recientes en la Cuenca de Almazán, *Rev. Soc. Geol. Esp.*, *10*(1-2), 183-196, 1997.

Cortés, A. L., and A. Maestro, Recent intraplate stress field in the eastern Duero Basin (N Spain), *Terra Nova*, *10*, 287-294, 1998.

Cortés, A. L., and J. L. Simón, Campos de esfuerzo recientes en la fosa de Alfambra-Teruel-Mira, in *Aportaciones al Conocimiento del Terciario Ibérico*, edited by J.P. Calvo and J. Morales, pp.65-68, Univ. Complutense de Madrid and Museo Nacional de Ciencias Naturales, Madrid, 1997.

Delouis, B., H. Haessler, A. Cisternas, and L. Rivera, Stress tensor determination in France and neighbouring regions, *Tectonophysics, 221*, 413-417, 1993.

De Ruig, D., Tectono-sedimentary evolution of the Prebetic fold belt of Alicante (SE Spain), Ph.D thesis, Vrije Univ., Amsterdam, 1992.

De Vicente, G., Análisis Poblacional de Fallas: El sector de enlace Sistema Central-Cordillera Ibérica, tesis doctoral, Univ. Complutense de Madrid, Madrid, 1988.

De Vicente, G., J. L. Giner, A. Muñoz-Martín, J. M. González-Casado, and R. Lindo, Determination of present-day stress tensor and neotectonic interval in the Spanish Central System and Madrid Basin, central Spain, *Tectonophysics, 266*, 405-424, 1996.

Dorbath, L., C. Dorbath, E. Jiménez, and L. Rivera, Seismicity and tectonic deformation in the eastern cordillera and the sub-Andean zone of the central Peru, *J. S. A. Earth Sci.*, *4*, 13-24, 1991.

Fuenzalida, H., L. Dorbath, A. Cisternas, H. Eyidogan, A. Barka, L. Rivera, H. Haessler, H. Philip, and N. Lyberis, Mechanism of the 1992 Erzincan earthquake and its aftershocks, tectonics of the Erzincan Basin and decoupling on the North Anatolian Fault, *Geophys. J. Int.*, *129*, 1-28, 1996.

Galindo-Zaldívar, J., F. González-Lodeiro, and A. Jabaloy, Stress and palaeostress in the Betic-Rif cordilleras (Miocene to the present), *Tectonophysics*, *227*, 105-126, 1993.

Galindo-Zaldívar, J., A. Jabaloy, I. Serrano, J. Morales, F. González-Lodeiro, and F. Torcal, Recent and present-day stresses in the Granada Basin (Betic Cordilleras): Example of a late Miocene-present-day extensional basin in a convergent plate boundary, *Tectonics, 18*, 686-702, 1999.

Giner, J. L., Análisis Neotectónico y Sismotectónico en el Sector Centro-Oriental de la Cuenca del Tajo, tesis doctoral, Univ. Complutense de Madrid, Madrid, 1996.

Goula, X., L. Talaya, A. Termens, I. Colomina, J. Fleta, B. Grellet, and T. Granier, Evaluació de la potencialitat sísmica del Pirineu Oriental, *Terra*, *28*(11), 41-58, 1996.

Goula, X., C. Olivera, J. Fleta, B. Grellet, R. Lindo, L.A. Rivera, A. Cisternas, and D. Carbon, Present and recent stress regime in the eastern part of the Pyrenees, *Tectonophysics*, *308*, 487-502, 1999.

Gregersen, S., Crustal stress regime in Fennoscandia from focal mechanisms, *J. Geophys. Res.*, *97*, 11,821-11,827, 1992.

Grellet, B., P. Combes, T. Granier and H. Philip, *Sismotectonique de la France Metropolitaine*, *Mem. Soc. Geol. Fr.*, vol.1, 76 pp., Mem. de la Soc. Geol.de Fr., Paris, 1993a.

Grellet, B., P. Combes, T. Granier and H. Philip, *Sismotectonique de la France Metropolitaine*, *Mem. Soc. Geol. Fr.*, vol.2, 24 maps, Mem. de la Soc. Geol.de Fr., Paris, 1993b.

Grünthal, G., and D. Stromeyer, The recent stress field in central Europe: Trajectories and finite

element modeling, *J. Geophys. Res.*, *97*, 11,805-11,820, 1992.

Herraiz, M., G. De Vicente, R. Lindo, and J. G. Sánchez- Cabañero, Seismotectonics of the Sierra Albarrana area (southern Spain): Constraints for a regional model of the Sierra Morena-Guadalquivir Basin limit, *Tectonophysics*, *266*, 425-442, 1996.

Herraiz, M. et al., Proyecto Sigma: Análisis del Estado de Esfuerzos Tectónicos, Reciente y Actual en la Península Ibérica, 240 pp., 2 maps, Cons. de Seguridad Nucl., Madrid, 1998.

Huibregtse, P.W., J. M. Van Alebeek, M. E. A. Zaal, and C. Biermann, Paleostress analysis of the Northern Nijar and Southern Vera basins: Constraints for the Neogene displacement history of mayor strike-slip faults in the Betic Cordilleras, SE Spain, *Tectonophysics, 300,* 79-101, 1998.

Instituto Geográfico Nacional (IGN), Análisis Sismotectónico de la Península Ibérica, Baleares y Canarias, *Pub. Tec. 26*, Madrid, 1992.

Jackson, J. A., and D. P. McKenzie, The relationship between plate motions and seismic moment tensor, and the rate of active deformation in the Mediterranean and Middle East, *Geophys. J., 93,* 45-73, 1988.

Julivert, M., J. M. Fontboté, A. Ribeiro, and L. E. Nabais Conde, Mapa Tectónico de la Península Ibérica y Baleares, map, scale 1:1,000,000, Inst. Geol. Miner. Esp., Madrid, 1972.

Klein, A., Hypocenter location program HYPOINVERSE; part I; Users guide to versions 1,2,3, and 4, *U.S. Geol. Surv., Open File Rep., 78-694*, pp. 65, 1978.

Lee, J. C., and J. Angelier, Paleostress trajectory maps based on the results of local determinations: The "lissage" program, *Comput. Geosci. 20*(2), 161-191, 1994.

Lindo, R., Sismotectonique des Andes du Perou Central: Apport des données sismologiques de haute précision, thèse de doctorat, Univ. Louis-Pasteur, Strasbourg, France, 1993.

Maestro, A., Las deformaciones alpinas en la Cuenca de Almazán (provincias de Soria y Zaragoza), tesis de licenciatura, Univ. de Zaragoza, Zaragoza, Spain, 1994.

Massana, E., L'activitat neotectonica a les Cadenes Costaneras Catalanes, tesis doctoral, Univ. de Barcelona, Barcelona, Spain, 1995.

Mercier, J. L., and E. Carey-Gailhardis, Regional state of stress and characteristic fault kinematics instabilities shown by aftershock sequences of the 1978 Thessaloniki (Greece) and 1980 Campania-Lucania earthquakes as examples, *Earth. Planet. Sci. Lett.*, *92*, 247-264, 1989.

Mezcua, J., and J. Rueda, Location of earthquakes under Iberia: Consequences of the ILIHA-DSSA data, *Monogr. 10,* pp. 251-262, Inst. Geogr. Nac., Madrid, 1993.

Mezcua, J., M. Herraiz, and E. Buforn, Study of the 6 June 1977 Lorca (Spain) earthquake and its aftershock sequence, *Bull. Seismol. Soc. Am., 74*, 167-180, 1984.

Müller, B., M. L. Zoback, K. Fuchs, L. Mastin, S. Gregersen, N. Pavoni, O. Stephansson, and C. Ljunggren, Regional patterns of tectonic stress in Europe, *J. Geophys. Res., 97,* 11,783-11,803, 1992.

Müller, B., V. Wehrle, H. Zeyen, and K. Fuchs, Short-scale variations of tectonic regimes in the western European stress province north of the Alps and Pyrenees, *Tectonophysics*, *275,* 199-219, 1997.

Olivera, C., T. Susagna, A. Roca, and X. Goula, Seismicity of the Valencia Trough and surrounding areas, *Tectonophysics*, *203*, 99-109, 1992.

Paricio, J., and J. L. Simón, Aportaciones al conocimiento de la compresión tardía en la Cordillera Ibérica Centro-Oriental: La cuenca neógena inferior del Mijares (Teruel-Castellón), *Estud. Geol., 42*, 302-319, 1986.

Philip, H., J. C. Bousquet, J. Escuer, J. Fleta, X. Goula, and B. Grellet, Presence de failles inverses d'âge quaternaire dans l'Est des Pyrénées: Implications sismotectoniques, C. R. Acad. Sci. Ser. II, 314, 1239-1245, 1991.

Rebaï, S., H. Philip, and A. Taboada, Modern tectonic stress field in the Mediterranean region: Evidence for variation in stress directions at different scales, *Geophys. J. Int.*, *110,* 106-140, 1992.

Reches, Z., Faulting of rocks in three-dimensional strain fields, II, Theoretical analysis, *Tectonophysics, 95,* 133-156, 1983.

Reches, Z., Determination of the tectonic stress tensor from slip along faults that obey the Coulomb yield condition, *Tectonics*, *6*, 849-861, 1987.

Reches, Z., G. Baer, and Y. Hatzor, Constraints on the strength of the upper crust from stress inversion of fault slip data, *J. Geophys. Res., 97,* 12,481-12,493, 1992.

Ribeiro, A., J. Cabral, R. Baptista, and L. Matías, Stress pattern in Portugal mainland and the adjacent Atlantic region, West Iberia, *Tectonics, 15*, 641-659, 1996.

Rivera, L. A., and A. Cisternas, Stress tensor and fault plane solutions for a population of earthquakes, *Bull. Seismol. Soc. Am., 80,* 600-614, 1990.

Sanz de Galdeano, C., La fracturación del borde sur de la Depresión de Granada (discusión acerca del escenario del terremoto del 25-XII-1884), *Estud. Geol.*, *41*, 59-68, 1985.

Simón, J. L., Late Cenozoic stress field and fracturing in the Iberian Chain and Ebro Basin (Spain), *J. Struct. Geol., 11*(3), 285-294, 1989.

Simón, J. L., and A. Soriano, La falla de Concud (Teruel): Actividad cuaternaria y régimen de esfuerzos asociado, in *El Cuaternario en España*, Vol. U, edited by T. Aleixandre and A. Pérez, pp., 729-737, Inst. Geol. Miner. Esp., Madrid, 1993.

Stapel, G., R. Moeys, and C. Biermann, Neogene evolution of the Storbas Basin (SE Spain) determined by paleostress analysis, *Tectonophysics*, *255*, 291-305, 1996.

Stuart, A., The Ideas of Sampling, Charles Griffin, London, 1984

Udías, A., and E. Buforn, Regional stresses along the Eurasia-Africa plate boundary derived from focal mechanisms of large earthquakes, in *Source Mechanism and Seismotectonics,* edited by A. Udías and E. Buforn, pp. 433-448, Birkhäuser Boston, Cambridge, Mass., 1991.

Vidal, F., Sismotectónica de la región de las Béticas-Mar de Alborán, tesis doctoral, Univ. de Granada, Granada, Spain, 1986.

Zoback, M. L., First- and second-order patterns of stress in the lithosphere: The World Stress Map project, *J. Geophys. Res.*, *97,* 11,703-11,728, 1992.

L. Cabañas, J. I. Cicuéndez, M. Herraiz, R. Lindo-Ñaupari, and O. Vadillo, Dpto. de Geofísica y Meteorología, F. CC. Físicas, Universidad Complutense de Madrid, 28040 Madrid, Spain. (mherraiz@eucmax.sim.ucm.es)

G. de Vicente, P. Rincón, and M. A. Rodríguez-Pascua, Dpto. de Geodinámica, F. CC. Geológicas, Universidad Complutense de Madrid, 28040 Madrid, Spain. (albosque@eucmax.sim.ucm.es)

J. Giner and J. M. González-Casado, Dpto. de Química Agrícola, Geología y Geoquímica, Universidad Autónoma de Madrid, 28049 Madrid, Spain. (g.casado@uam.es)

A. Casas, A. L. Cortés, and J. L. Simón, Dpto. de Geología, Universidad de Zaragoza, Plaza de San Francisco s/n, 50009 Zaragoza, Spain. (acortes@posta.unizar.es)

M. Ramírez, Consejo de Seguridad Nuclear, c/Justo Dorado, 11, 28040 Madrid, Spain.

M. Lucini, Empresa Nacional de Residuos Radiactivos, S.A., c/Emilio Vargas, 7, 28043 Madrid, Spain.

(Received July 23, 1999;
revised January 5, 2000;
accepted January 11, 2000.)